Large-scale genome editing based on high-capacity adenovectors and CRISPR-Cas9 nucleases rescues full-length dystrophin synthesis in DMD muscle cells

Tasca, F.; Brescia, M.; Wang, Q.; Liu, J.; Janssen, J.M.; Szuhai, K.; Goncalves, M.A.F.V.

Published online 1 July 2022

Nucleic Acids Research, 2022, Vol. 50, No. 13 ***7761–7782***
https://doi.org/10.1093/nar/gkac567

Large-scale genome editing based on high-capacity adenovectors and CRISPR-Cas9 nucleases rescues full-length dystrophin synthesis in DMD muscle cells

Francesca Tasca[1], Marcella Brescia[1,2], Qian Wang[1], Jin Liu[1], Josephine M. Janssen[1], Karoly Szuhai[1] and Manuel A.F.V. Gonçalves[1,*]

[1]Department of Cell and Chemical Biology, Leiden University Medical Center, Einthovenweg 20, 2333 ZC, Leiden, The Netherlands and [2]Department of Anatomy and Embryology, Leiden University Medical Center, Einthovenweg 20, 2333 ZC Leiden, The Netherlands

Received January 14, 2022; Revised May 20, 2022; Editorial Decision June 16, 2022; Accepted June 20, 2022

ABSTRACT

Targeted chromosomal insertion of large genetic payloads in human cells leverages and broadens synthetic biology and genetic therapy efforts. Yet, obtaining large-scale gene knock-ins remains particularly challenging especially in hard-to-transfect stem and progenitor cells. Here, fully viral gene-deleted adenovector particles (AdVPs) are investigated as sources of optimized high-specificity CRISPR-Cas9 nucleases and donor DNA constructs tailored for targeted insertion of full-length dystrophin expression units (up to 14.8-kb) through homologous recombination (HR) or homology-mediated end joining (HMEJ). In muscle progenitor cells, donors prone to HMEJ yielded higher CRISPR-Cas9-dependent genome editing frequencies than HR donors, with values ranging between 6% and 34%. In contrast, AdVP transduction of HR and HMEJ substrates in induced pluripotent stem cells (iPSCs) resulted in similar CRISPR-Cas9-dependent genome editing levels. Notably, when compared to regular iPSCs, in p53 knockdown iPSCs, CRISPR-Cas9-dependent genome editing frequencies increased up to 6.7-fold specifically when transducing HMEJ donor constructs. Finally, single DNA molecule analysis by molecular combing confirmed that AdVP-based genome editing achieves long-term complementation of DMD-causing mutations through the site-specific insertion of full-length dystrophin expression units. In conclusion, AdVPs are a robust and flexible platform for installing large genomic edits in human cells and p53 inhibition fosters HMEJ-based genome editing in iPSCs.

GRAPHICAL ABSTRACT

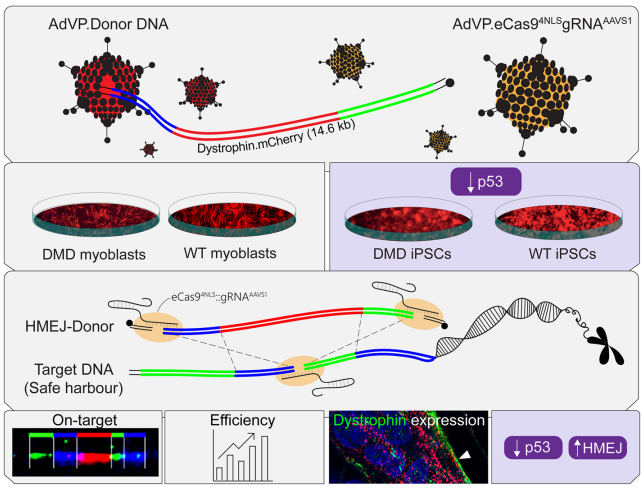

INTRODUCTION

Genome editing is a fast-evolving field with increasing impact in basic science, biotechnology and medicine (1,2). Particularly versatile genome editing strategies permit incorporating exogenous donor sequences into endogenous loci subjected to double-strand DNA breaks (DSBs) made by engineered CRISPR-Cas9 nucleases (3–9). This versatility stems from the amenability of these gene knock-in strategies to genomic modifications spanning from single base-pairs to entire transgene(s); and from the straightforward designing of CRISPR-Cas9 nucleases with high activities and specificities (3–9). Indeed, in contrast to earlier programmable nucleases, CRISPR-Cas9 nucleases are assembled in a protein engineering-free manner, in that they consist of sequence-customizable guide RNAs (gRNAs) and immutable RNA-programmable Cas9 proteins that cleave target sequences upon gRNA–DNA hybridization (9,10). Hence, targeted DNA knock-ins can be

*To whom correspondence should be addressed. Tel: +31 71 5269238; Fax: +31 71 5268270; Email: m.f.v.goncalves@lumc.nl

accomplished by delivering CRISPR-Cas9 nucleases together with donor DNA constructs whose designs favor site-specific DSB repair through either; non-homologous end joining (NHEJ) or homology-directed repair (HDR) pathways (11,12), i.e. homologous recombination (HR), microhomology-mediated end joining (MMEJ) and, more recently, homology-mediated end joining (HMEJ) (13,14). In contrast to the lack of homology to target sequences in NHEJ-prone donors (15,16), MMEJ, HMEJ and HR donors present increasingly larger homology tracts flanking the foreign DNA of interest, with each homology arm typically spanning 20–30 bp, ∼900 bp and 0.5–2.0 kb, respectively. Moreover, diversely from HR donors, donors tailored for ectopic NHEJ, MMEJ and HMEJ, have their targeting modules flanked by CRISPR-Cas9 cleaving sites. This 'double-cut' arrangement ensures exogenous DNA release from construct backbones in cell nuclei, fostering gene knock-ins via the processing and alignment of donor and target DNA termini (11,12).

When compared to NHEJ and MMEJ donors, more exact and properly oriented chromosomal integration of exogenous DNA is achieved through HMEJ and HR donor designs (15). In addition, it is well-established that the efficiency and precision of ectopic HR profits from extending homology tracts especially when aiming at chromosomal insertion of larger genetic payloads (13,17,18). Normally, HMEJ donors yield higher gene knock-in frequencies than HR, NHEJ or MMEJ donors (13,14), however, the performance of HMEJ donors containing homology lengths considerably longer than the typical ∼900-bp, has not been assessed. Equally of notice, HMEJ-based genome editing, similarly to other strategies based on 'double-cut' donors, can take place in HR refractory non-dividing cells, turning it into a high-potential approach for *in vivo* applications (14,19). Notwithstanding, unwanted chromosomal insertion of prokaryotic backbone sequences is associated with donor plasmid delivery, especially when applying the 'double-cut' genome editing strategies (20). Critically, plasmids harbouring large transgenes and/or large homology tracts transfect poorly even in easy-to-transfect cells which, often, demands complex and time-consuming cell selection procedures.

Viral vectors instead achieve efficient delivery of genome editing tools into hard-to-transfect cell types (21). However, commonly used adeno-associated viral vectors cannot deliver large transgenes nor large homology tracts due to their limited packaging capacity (<4.7 kb) (21,22). There is, therefore, a pressing need for alternative DNA delivery systems allowing the efficacious investigation and application of novel genome editing principles independently of the size of the attendant tools. In this regard, high-capacity adenoviral vectors (also named third-generation adenoviral vectors), henceforth dubbed adenovector particles (AdVPs), congregate a valuable set of features: (i) lack of viral genes; (ii) vast packaging capacity (up to 36 kb); (iii) high genetic stability; (iv) amenability to straightforward cell-tropism modifications; and (v) efficient transduction of dividing and non-dividing cells (23–25).

Here, we demonstrate that AdVPs are suitable for engineering large-scale genomic edits in human stem and progenitor cells upon the delivery of optimized high-specificity CRISPR-Cas9 nucleases and donor constructs tailored for HR or HMEJ. In parallel, these tools were applied for testing the rescue of the genetic defect underlying Duchenne muscular dystrophy (DMD) in human myogenic cells, i.e. muscle progenitor cells (myoblasts) and induced pluripotent stem cells (iPSCs). DMD (MIM #310200) is a lethal and frequent muscle-wasting X-linked disorder (prevalence: ∼1 in 4700 boys) caused by a multitude of diverse types of mutations scattered along the enormous *DMD* gene (∼2.4 Mb). These mutations disrupt striated muscle-specific dystrophin isoforms (427-kDa) encoded in 14-kb mRNA transcripts with 79 exons (26). The absence of cytoskeleton-to-dystrophin glycoprotein complex (DGC) linkages in muscle cells results in sarcolemma fragility and impaired cell signalling. Eventually, this leads to the replacement of damaged muscle with fibrotic and adipose tissues (26). Currently, the vast majority of DMD-directed genetic therapies are mutation-specific and/or yield only partially functional micro-dystrophins or shortened Becker-like dystrophins (26,27). Complementation of DMD-causing mutations regardless of their type or location via stable expression of full-length dystrophin offers the perspective for more effective and broadly applicable approaches, including those involving *ex vivo* correction and autologous transplantation of stem/progenitor cells with myogenic capacity (28,29).

Notably, iPSCs represent a particularly valuable cell source for the development of DMD-targeting genetic therapies (28,29). Indeed, iPSCs derived from reprogrammed human somatic cells are capable of unlimited self-renewal *in vitro* and, under proper stimuli, differentiate into specific cell types (30), including skeletal and cardiac muscle cells. These features support *in vitro* disease modelling and, in combination with genome editing technologies, the development of candidate autologous cell therapies. Genome editing of iPSCs mostly involves the introduction of genetic changes encoded in oligonucleotide or plasmid DNA substrates. The former substrates can yield small but high-frequency genomic edits; the latter, in contrast, normally require linkage to laborious positive-selection genes whose removal depends on laborious supplementation of site-specific recombinases or transposases. Critically, homology-directed installation of larger edits renders the iPSC genome editing process even more challenging due to the difficulty in transferring the correspondingly sizable genetic payloads into these cells in an efficient and non-cytotoxic manner (9,10).

In this study, we show that AdVP delivery of donors prone to HMEJ or HR, together with matched CRISPR-Cas9 complexes, achieves targeted integration of transgenes encoding full-length, hence fully functional, dystrophin in HeLa cells, myoblasts and iPSCs. In myoblasts, HMEJ donors led to significantly higher frequencies of site-specific transgene integration than HR donors. Via additional AdVP transduction experiments, we further found that HMEJ-based genome editing is compromised in iPSCs yet, it can be enhanced via p53 inhibition. Importantly, edited myoblasts kept stable recombinant full-length dystrophin protein synthesis and differentiation capability. Finally, we confirmed that CRISPR-Cas9-dependent stable full-length dystrophin expression is, in most cases, the result of the precise chromosomal insertion of HMEJ and HR

donor sequences at a commonly used safe harbour locus, i.e. the adeno-associated virus integration site 1 (*AAVS1*) at 19q13.4-qter.

MATERIALS AND METHODS

Cells

Human cervix carcinoma HeLa cells (American Type Culture Collection) were cultured in Dulbecco's modified Eagle's medium (DMEM; Thermo Fisher Scientific; Cat. No.: 41966-029) supplemented with 5% (v/v) fetal bovine serum ultra-low endotoxin (FBS; Biowest; Cat. No.: S1860-500). The origins of and culture conditions for the human wild-type myoblasts (31) as well as for the *DMD*-defective myoblasts, herein referred to as myoblasts DMD.A (32) and DMD.B (31) have been previously described (33). In brief, the cells were grown in Skeletal Muscle Cell Growth Medium (Ready-to-use; PromoCell; Cat. No.: C-23060) supplemented with 20% FBS, 1 × Glutamax (Thermo Fisher Scientific; Cat. No.: 35050–061) and 100 U ml^{-1} penicillin/streptomycin (Thermo Fisher Scientific; Cat. No.: 15140-122). The *DMD*-defective human induced pluripotent stem cells (iPSCs) used in this work, CENSOi001-B (herein referred to as DMD iPSCs), were purchased from the European Bank for induced pluripotent Stem Cells (EBiSC). The generation and characterization of the wild-type iPSCs LUMC0020iCTRL (34,35) and LUMC0072iCTRL01 (36), were detailed elsewhere. The iPSCs were cultured in mTeSR medium (STEMCELL Technologies; Cat. No.: 85850) or in feeder-free Essential 8 Medium (E8; ThermoFisher Scientific; Cat. No.: A1517001) both supplemented with 25 U ml^{-1} penicillin and 25 μg ml^{-1} of streptomycin. The DMD iPSCs were cultured in plates coated with Matrigel (Corning Matrigel hESC-Qualified Matrix; Corning; Cat. No.: 354277) when cultured with mTeSR medium or in plates coated with Vitronectin Recombinant Human Protein (VTN-N; ThermoFisher Scientific; Cat. No.: A14700) when cultured with E8 medium according to the manufacturer guidelines. When ready for sub-culturing, to let cell-cell dissociation occur, the iPSCs were washed with phosphate-buffered saline (PBS; pH 7.4) solution and then incubated with 0.5 mM ethylenediaminetetraacetic acid (EDTA; Invitrogen Cat. No.: 15575020) in PBS at 37°C for 5 min. After the removal of the EDTA solution, the cells were seeded in new wells with the proper medium supplemented with a 1:200 dilution of the ROCK inhibitor-containing solution RevitaCell (ThermoFisher Scientific; Cat. No.: A2644501). The PEC3.30 AdVP packaging cells (33) were kept in high-glucose DMEM supplemented with 10% FBS, 10 mM $MgCl_2$ and 0.4 μg ml^{-1} puromycin (Thermo Fisher Scientific; Cat. No.: A11138-03). Finally, HEK293T cells were maintained in DMEM supplemented with 10% FBS and 100 U ml^{-1} penicillin/streptomycin. The cells used in this study were mycoplasma-free and were kept at 37°C in humidified-air atmospheres with 10% CO_2 (HeLa cells, HEK293T) or 5% CO_2 (Myoblasts and iPSCs) and at 39°C in humidified-air atmospheres with 10% CO_2 (PEC3.30 cells).

Production and characterization of adenoviral vectors

The constructs AO75_pHC.Ad.EGFP::DYS, AQ77_pHC.Ad.EGFP::DYS^{TS}, BE14_pHC.Ad.DYS.mCherry, BE15_pHC.Ad.DYS.$mCherry^{TS}$ and AX70_pHC.Ad.$eCas9^{4NLS}gRNA^{S1}$ were the molecular clones used for the production of the fiber-modified AdVPs AdVP.EGFP::DYS, AdVP.EGFP::DYS^{TS}, AdVP.DYS.mCherry, AdVP.DYS.$mCherry^{TS}$ and AdVP.$eCas9^{4NLS}gRNA^{S1}$ respectively. The annotated maps and nucleotide sequences of the AdVP genomes are available in the Supplementary Information. The construct encoding the human full-length dystrophin fused to EGFP (EGFP::DYS) and the construct containing the synthetic 436-bp striated muscle-specific *CK8* promoter were detailed elsewhere (37,38). The protocols used in the generation and purification of the resulting fiber-modified AdVP stocks have been described in detail before (33). In brief, the bacteriophage P1 Cre recombinase- and adenovirus type 5 E1-expressing PEC3.30 producer cells, were seeded at a density of 1.4×10^6 cells per well of 6-well plates (Greiner Bio-One) one day prior to transfection in medium deprived of puromycin. Subsequently, 6.25 μg of MssI-linearized AO75_pHC.Ad.EGFP::DYS or AQ77_pHC.Ad.EGFP::DYS^{TS} were diluted in a total volume of 200 μl of 150 mM NaCl to which were added 20.6 μl of a 1 mg ml^{-1} solution of 25-kDa linear polyethyleneimine (PEI; Polysciences). After vigorous mixing in a vortex for about 10 sec, the solutions were incubated for 25 min at room temperature (RT) to let DNA-PEI complexes form. Finally, the DNA-PEI complexes were directly added to the medium of the producer cells. Six hours later, the transfection medium was substituted by fresh medium containing *E1*-deleted helper AdV vector AdV.SRα.LacZ.1.50 (39) at a multiplicity of infection (MOI) of 7.5 infections units (IU) per cell. The helper vector drives the expression of the proteins necessary for the replication and assembly of the AdV particles. In addition, the PEC3.30 cells express a thermosensitive version of the adenovirus DNA-binding protein (DBP) that further contributes to vector complementation once producer cells are placed at the permissive temperature of 34°C. Upon helper-triggered emergence of about 80–100% of cytopathic effect (CPE), producer cells were harvested and subjected to three cycles of freezing and thawing in liquid N_2 and 37°C water baths, respectively. Next, cellular debris was removed by centrifugation for 10 min at 2000 × g and supernatants containing the vector particles were collected. Assembled vector particles present in the clarified supernatants were subsequently amplified through four rounds of propagation in producer cells transduced with helper AdV.SRα.LacZ.1.50. The last round of propagation involved seventeen T175-cm^2 culture flasks. The resulting AdV particles were then purified by sequential block and continuous CsCl buoyant density ultracentrifugation steps and were de-salted by ultrafiltration through Amicon Ultra-15 100K MWCO filters (MerckMillipore; Cat. No.: UFC910024). The production of AdVP.DYS.mCherry, AdVP.DYS.$mCherry^{TS}$ and AdVP.$eCas9^{4NLS}gRNA^{S1}$ involved essentially the same procedure applied for the production of AdVP.EGFP::DYS,

AdVP.EGFP::DYS^{TS}, except that 1.6×10^6 PEC3.30 cells per well were seeded for the initial transfection step and, six hours later, the transfection media were substituted by fresh media containing helper AdV.SRα.LacZ.1.50 at an MOI of 30 IU cell^{-1}. The functional titers of the purified AdVP stocks AdVP.EGFP::DYS, AdVP.EGFP::DYS^{TS}, AdVP.DYS.mCherry, and AdVP.DYS.mCherry^{TS} were calculated by transducing HeLa cells with a range of vector stock dilutions. Three days post-transduction the percentages of reporter-positive cells were evaluated through flow cytometry. The resulting titers were 5.23×10^8 HeLa-transducing units (TU) ml^{-1}, 3.92×10^8 TU ml^{-1}, 7.38×10^{10} TU ml^{-1} and 7.42×10^{10} TU ml^{-1} for AdVP.EGFP::DYS, AdVP.EGFP::DYS^{TS}, AdVP.DYS.mCherry, and AdVP.DYS.mCherry^{TS}, respectively. The titer of AdVP.eCas9^{4NLS}gRNA^{S1} was assessed by using the Quant-iT™ PicoGreen™ dsDNA Assay Kit reagents (Thermo Fisher Scientific; Cat. No.: P11496A) as detailed elsewhere (39). The resulting titer of AdV.Cas9.gRNA^{S1} was 2.82×10^{12} genome copies (GC) ml^{-1}. In addition, the AdVP physical titers were also determined through qPCR assays. Firstly, the vector DNA was isolated from purified AdVP stocks by using the DNeasy Blood & Tissue kit (QIAGEN; Cat. No.: 69506) and diluted 1:100. Next, three 3-fold serial dilutions of the extracted vector genomes were employed for qPCR using the iQ™ SYBR® Green Supermix (Bio-Rad; Cat. No.: L010171C) and the primers targeting the AdVPs packaging signal (ψ) listed in Supplementary Table S1. As standard curve 8 serial 10-fold dilutions of a linearized parental plasmid stock containing 1×10^7 GC μl^{-1} was used as qPCR template. The qPCR primers, cycling conditions and components are specified in Supplementary Tables S1 and S2. Data analysis was performed by using the Bio-Rad CFX Manager 3.1 software and the titers were calculated based on the Ct values of standard curve and viral vector dilutions. The physical and functional AdVP titers are summarized in Supplementary Table S3. The structural integrity of vector genomes packaged in purified adenoviral capsids was carried out essentially as described previously (33). In brief, 80–100 μl of purified AdVPs were treated with 8 μl of 10 mg ml^{-1} DNaseI (Sigma-Aldrich; Cat. No.: 10104159001) at 37 °C for 30 min. Next, the DNase I was inactivated by adding 2.4 μl of 0.5 M EDTA solution (pH 8.0), 6 μl of 10% (w/v) sodium dodecyl sulphate (SDS) and 1.5 μl of 20 mg ml^{-1} proteinase K (Thermo Fisher Scientific; Cat. No.: EO0491). The resulting mixtures were then incubated at 55 °C for 1 h and vector DNA isolation was completed by using the QIAEX II Gel Extraction Kit (QIAGEN; Cat. No.: 20021) following the manufacturer's instructions. Finally, the isolated vector genomes were subjected to restriction enzyme fragment analysis (RFLA) by using the Gel-Doc XR+ system (Bio-Rad) and the Image Lab 6.0.1 software (Bio-Rad). Parental plasmids, digested with the same restriction enzymes applied to vector genomes, served as molecular weight references. The *in-silico* restriction patterns corresponding to intact plasmid and vector DNA were made with the aid of SnapGene (version 5.2.4) software.

Production of lentiviral vectors

The oligonucleotide pairs used for assembling lentiviral vector transfer plasmids pLV.Neo.shp53 and pLV.Neo.shLacZ encoding shRNAs shp53 and shLacZ, respectively, are listed in Supplementary Table S4. After annealing, the oligonucleotide pairs were inserted through cohesive end ligation into the BbsI- and XhoI-treated expression cassette from a previously published doxycycline-regulated lentiviral vector system harbouring a *TetO*-modified human *H1* promoter (40). The corresponding lentiviral vectors LV.Neo.shp53 and LV.Neo.shLacZ were generated according to previously detailed protocols (41,42). In brief, one day prior to transfection HEK293T cells were seeded in 175-cm^2 culture flasks (Greiner Bio-One). Next, 30 μg of DNA composed of lentiviral vector shuttle, packaging, and VSV-G-pseudotyping plasmids at a ratio of 2:1:1 (size-normalized for molecule copy number) and 90 μl of 1 mg ml^{-1} PEI solution (25 kDa PEI; Polysciences) were diluted in 1 ml of a 150 mM NaCl solution. Upon vigorous mixing in a vortex for about 10 sec and incubation for 25 min at RT, the DNA-PEI complexes were directly added to the medium of the producer cells. The packaging and pseudotyping constructs used were psPAX2 (Addgene #12260) and pLP/VSVG (Invitrogen), respectively. After 24 hours the transfection medium was replaced by fresh DMEM supplemented with 5% FBS. At 3 days post-transfection, the producer-cell conditioned medium was harvested, and the cellular debris was removed by centrifugation and filtration through 0.45-μm pore-sized HT Tuffryn membrane filters (Pall Life Sciences; Cat. No.: PN4184). The lentiviral vector particle titers in the clarified supernatants were assessed by employing the RETROTEK HIV-1 p24 antigen ELISA kit (ZeptoMetrix; Cat. No.: 0801111). The resulting titers for LV.Neo.shp53 and LV.Neo.shLacZ were 590 ng p24^{gag} ml^{-1} and 660 ng p24^{gag} ml^{-1}, respectively.

Generation of p53 knockdown iPSCs

The generation of DMD iPSCs and wild-type iPSCs conditionally expressing a short hairpin RNA (shRNA) controlling p53 downregulation, shp53, was initiated by lentiviral vector transduction with LV.Neo.shp53. As control, parallel cell cultures were transduced with LV.Neo.shLacZ expressing a shRNA targeting *LacZ*, shLacZ. These lentiviral vectors encode a neomycin-resistance gene (*Neo*^{R}) and the shRNAs under the control of a doxycycline-inducible promoter. In brief, cells were seeded in regular growth medium at a density of 6×10^4 cells per well of 24-well plates. The following day DMD iPSCs and wild-type iPSCs (LUMC0020iCTRL) were exposed to medium containing each lentiviral vector at an MOI of 1 and 0.1 TU ml^{-1}, respectively. After three days, the cells were transferred to a new plate containing regular growth medium and one day later, the medium was supplemented with 50 μg ml^{-1} of G418 sulfate (Millipore; Cat. No.: 345810). Parental mock-transduced cells served as negative controls during the drug selection procedure. The resulting stably transduced iPSCs were cultured in medium supplemented with 10 ng ml^{-1} doxycycline (Sigma-Aldrich; Cat. No.: D9891)

to activate p53 downregulation as confirmed through western blot analysis. To activate shRNA expression, doxycycline was added three days prior to the start of the AdVP transduction experiments and was kept throughout the duration of these experiments.

Quantitative polymerase chain reaction (qPCR)

Episomal donor DNA amounts were traced through *EGFP*-directed qPCR analysis. In brief, HeLa cells were transduced with AdVP.EGFP::DYS and AdVP.EGFP::DYS^{TS} alone, at an MOI of 8 TU ml^{-1}, or together with AdVP.eCas9^{4NLS}gRNA^{S1} at an MOI of 3×10^3 GC cell^{-1}. Next, DNA was extracted at 3-, 12-, and 28-days post-transduction with the DNeasy Blood & Tissue kit (QIAGEN; Cat. No.: 69506). Extracted DNA from mock- and AdVP-transduced cells was subsequently subjected to qPCR using the iQ™ SYBR® Green Supermix (Bio-Rad; Cat. No.: L010171C) together with the primers targeting *EGFP* and *GAPDH* listed in Supplementary Table S1. The cycling conditions and components of qPCR mixtures are specified in Supplementary Tables S1 and S2. The signal outputs were detected by using the CFX Connect Real-Time PCR Detection System (Bio-Rad) and the resulting data was analysed via the Bio-Rad CFX Manager 3.1 software.

Reverse transcriptase-qPCR (RT-qPCR)

The knockdown of*TP53* expression, resulting in downregulation of the p53 target genes *p21*, *PUMA* and *FAS*, was assessed by RT-qPCR analysis of cells expressing shp53 incubated for at least two days in the presence of 10 ng ml^{-1} doxycycline (Sigma-Aldrich; Cat. No.: D9891). Cells expressing shLacZ instead of shp53 served as control. Total RNA from cell cultures was extracted by using the NucleoSpin RNA kit essentially according to the manufacturer's instructions (Macherey Nagel; Cat. No.: 740955). Next, reverse transcription was conducted with the SuperScript III Reverse Transcriptase Kit (Invitrogen; Cat. No.: 18080–044). In brief, 1000 ng of RNA was incubated with 1 μl of 100 ng μl^{-1} random primers and 1 μl of 10 mM dNTPs mixed in a 13-μl reaction volume. The reaction mixtures were incubated for 5 min at 65°C followed by 2 min at 4°C. Next, to each tube was added 4 μl 5× First-Strand Buffer, 2 μl of 20 U ml^{-1} RiboLock RNase Inhibitor (Thermo Fisher Scientific; Cat. No.: EO0381), 1 μl 0.1 M DTT and 1 μl of SuperScript™ III RT (200 units μl^{-1}). Finally, the samples were incubated at 25°C for 5 min followed by incubation at 50°C for 1 h. Eventually, the reactions were terminated by heating at 70°C for 15 min. The resulting cDNA templates were then diluted 5-fold in nuclease-free water and 1-μl samples of diluted cDNA were subjected to qPCR by using the iQ™ SYBR® Green Supermix (Bio-Rad; Cat. No.: L010171C) and the primers listed in Supplementary Table S1. *GAPDH* transcripts served as RT-qPCR targets for gene expression normalization. The signal outputs were detected by using the CFX Connect Real-Time PCR Detection System (Bio-Rad) and data analysis was performed using Bio-Rad CFX Manager 3.1 software. The qPCR mixture components and cycling conditions are specified in Supplementary Tables S1 and S2, respectively.

Transduction experiments

Transduction experiments in HeLa cells and human myoblasts were initiated by seeding the cells in wells of 24-well plates at a density of 4×10^4 and 5×10^4 cells per well, respectively. The next day, the cells were incubated in 500 μl of medium containing AdVPs at different MOI. Transduction efficiencies were determined at 3 days post-transductions by reporter-directed flow cytometry and direct fluorescence microscopy analyses. Transduction experiments in iPSCs were performed as follows. RevitaCell was added at a dilution of 1:200 to the cells for 30 minutes prior to the transfer procedure to maximize cell survival. The cells were dissociated to obtain cell suspensions having 1×10^5 cells in 100 μl of medium supplemented with RevitaCell (1:200). The cell suspensions were subsequently added to a V-bottom 96-well plate (Greiner Bio-One) containing AdVPs in 100 μl of medium. After 1 hour of incubation at 37°C in a humidified-air atmosphere with 5% CO_2, the cells were transferred to a 12-well plate containing medium supplemented with RevitaCell (1:200). Two hours later, fresh medium supplemented with RevitaCell (1:200) was added. Transduction efficiencies were assessed at 3- or 4-day post-transduction by reporter-directed flow cytometry and direct fluorescence microscopy analyses.

Cell differentiation assays

The human myoblasts were transferred in a regular culture medium into wells pre-coated with a 0.1% (w/v) gelatin solution (Sigma-Aldrich; Cat. No.: G13393). After reaching full confluency, the muscle progenitor cells were exposed to myogenic differentiation medium consisting of phenol red-free DMEM (ThermoFisher Scientific; Cat. No.: 11880–028) supplemented with 100 μg ml^{-1} human holo-transferrin (Sigma-Aldrich; Cat. No.: T0665), 10 μg ml^{-1} human insulin (Sigma-Aldrich; Cat. No.: I9278) and 100 U ml^{-1} penicillin/streptomycin. Post-mitotic myotubes were detected 4–6 days later by immunofluorescence staining and western blot analyses with antibodies specific for the late muscle-specific markers sarcomeric α-actinin and myosin heavy-chain. The differentiation of iPSCs along the three embryonic germ layers was induced by using a spontaneous differentiation protocol as follows. The iPSCs were first treated with 0.5 mM EDTA in PBS for 1 min at 37°C and were subsequently gently dissociated into large cell clumps by scrapping. The resulting cell clumps were then cultured in suspension for 24 h on low-attachment plates at 37°C. Next, the iPSCs were seeded on glass coverslips coated with VTN-N in E8 medium containing RevitaCell (1:200) and, the following day, this medium was substituted by DMEM/F12 growth medium (Thermo Fisher Scientific; Cat. No.: 31331–028) containing 20% FBS. The DMEM/F12 medium was replenished every 2–3 days. After 3 weeks under differentiation conditions, the iPSCs were processed for confocal immunofluorescence microscopy for the detection of markers characteristic of the endoderm, mesoderm and ectoderm lineages. The markers tested were α-fetoprotein (AFP), forkhead box protein A2 (FOXA2), α-smooth muscle actin (α-SMA), endothelial cell adhesion molecule-1 (CD31), and tubulin β3 class III (TUBB3). The cardiomyogenic differentiation of iPSCs was carried out fol-

lowing the protocol for cardiac lineage differentiation based on stepwise supplementation of iPSC medium with specific small molecules as described elsewhere (43). In brief, iPSCs kept in E8 medium supplemented with RevitaCell (1:200) were seeded in 12-well plates coated with Matrigel (Corning; Cat. No.: 734–1440) or Geltrex (ThermoFisher; Cat. No.: A1413301) at different cell densities, ranging from 5×10^4 to 9×10^5 cells. At 24 h after seeding, the medium was replaced with modified LI-BPEL (mBEL) medium (43) supplemented with 5 μM CHIR 99021 (Axon Medchem; Cat. No.: Axon1386). Two days later, the medium was replenished with mBEL medium supplemented with 5 μM XAV 939 (Tocris; Cat. No.: 3748/10) and 0.25 μM IWP-L6 (AbMole; Cat. No.: M2781). Finally, after an additional 2-day period the medium was replenished with mBEL medium supplemented with Insulin-Transferrin-Selenium-Ethanolamine (ITS -X) (1:1000) (ThermoFisher; Cat. No.: 51500056). Next, the cells were kept in culture under differentiation conditions for up to 30–35 days in the presence of mBEL medium supplemented with ITS-X (1:1000) that was replenished every 2–3 days. Areas of beating cardiomyocytes were detected from day 10 onwards. Finally, at the selected differentiation endpoints, the detection of the tissue-specific markers cardiac troponin I (cTnI) and sarcomeric α-actinin was performed by immunofluorescence microscopy analyses.

Flow cytometry

Cell transduction frequencies were determined by reporter-directed flow cytometry using a BD LSR II flow cytometer (BD Biosciences). In brief, HeLa cells and human myoblasts were washed with PBS and, after trypsin treatment and centrifugation at 300 × g for 5 min, they were collected in PBS containing 0.5% BSA and 2 mM EDTA (pH 8.0) (FACS buffer). iPSCs were washed with PBS and treated with 0.5 mM EDTA in PBS for 5 min at 37°C for gentle dissociation. To obtain single-cell suspensions, the cells were collected by centrifugation at 200 × g for 2 min and were then resuspended in 200 μl of Accutase (STEMCELL Technologies; Cat. No.: 07920) and incubated for 10 min at 37°C. After centrifugation at 300 × g for 5 min, iPSCs were also resuspended in FACS buffer. Mock-transduced cells served as controls to establish background fluorescence levels. Data were analysed with the aid of FlowJo 10.6.0 software (TreeStar).

Chromosomal DNA content analysis

The DNA content in iPSCs with regular or knocked-down p53 levels genetically modified via HR- or HMEJ-based genome editing strategies, was assessed as follows. After the addition of 200 μl of Accutase (STEMCELL Technologies; Cat. No.: 07920), the cells were incubated for 10 min at 37°C to obtain single-cell suspensions. Next, after centrifugation at 300 × g for 5 min, the cells were resuspended in 70% ethanol and incubated at 4°C overnight. After one wash with PBS, the cells were resuspended in PBS containing 50 μg ml^{-1} RNAse A (ThermoFisher; Cat. No.: EN0531) and 20 μg ml^{-1} propidium iodide (Abcam; Cat. No.: ab14083). Finally, after an overnight incubation period at 4°C the four iPSC populations were washed twice with PBS, resuspended in FACS buffer, and analysed for ploidy number by propidium iodide-directed flow cytometry.

COBRA-FISH karyotyping of iPSCs

Combined binary ratio labelling multicolour FISH-based molecular karyotyping (COBRA-FISH) was performed to determine the karyotype of iPSCs with regular or knocked-down p53 levels genetically modified via HR- or HMEJ-based genome editing strategies. The detailed COBRA-FISH protocol applied to these cells has been published (44). In brief, metaphase suspensions were dropped on microscopy glass slides and airdried overnight. Slides with metaphase chromosomes were pre-treated at 37 ºC for 10 min with 100 μg ml^{-1} RNase A (Roche; Cat. No.: 10154105103) in 2 × saline-sodium citrate (SSC; Sigma-Aldrich; Cat. No.: S0902) and were then incubated with 0.005% pepsin (Sigma-Aldrich; Cat. No.: P0525000) in 0.1 M HCl for 5 min at 37 ºC. After a 10-min fixation at RT with 1% (v/v) formaldehyde (Merck; Cat. No.: 1.03999.1000) in PBS (pH 7.4), the specimens were dehydrated by three 3-min incubations in ethanol at increasing concentrations, i.e. 70%, 90% and 100%. Next, the coverslips were air-dried and exposed to whole-chromosome painting probes fluorescently labelled with the dyes 7-diethylaminocoumarin-3-carboxylic acid (DEAC), Cy3, Cy5 and rhodamine green by using the Universal Linkage System (ULS) kit (Kreatech Biotechnology). After DNA denaturation at 80°C for 75 s, hybridizations were let to proceed for 3 days at 37°C in a humidified chamber. Unbound probes were eliminated by first washing with 0.1% Tween-20 (Promega; Cat. No.: PRH5152) in 2 × SSC, and then with 50% formamide (Merck; Cat. No.: 1.09684.1000) in 2 × SSC pH 7.0 at 44 ºC followed by incubation at 60 ºC in 0.1 × SSC. Each washing step was done twice for 5 min. After dehydration by exposure to the above-mentioned increasing concentrations of ethanol, the specimens were air-dried and embedded in Citifluor AF1/DAPI (400 ng ml^{-1}) solution (Aurion; Cat. No.: E17970). Stained chromosomes were visualised with a Leica DMRA fluorescence microscope (Leica, Wetzlar, Germany) and images were captured with the aid of a CoolSnap HQ2 camera (Photometrics, Tucson, USA). A minimum of 35 metaphase cells were analysed from each sample and reported in the International System for Human Cytogenomic Nomenclature (ISCN) format.

Cell sorting and clonal expansion

Sorting of genetically modified cells was done using a BD FACS Aria III flow cytometer (BD Biosciences), following the removal of episomal DNA through sub-culturing of transduced myoblasts and iPSCs. The retrieved reporter-positive cells were collected in a 1:1 mixture of regular medium and FBS. Single cell-derived iPSC colonies were isolated by seeding at low-density single-cell suspensions of mCherry-positive cells in wells of 6-well plates containing culture medium supplemented with Revitacell (1:200), 50 μM α-thioglycerol and 20 nM of cathocuprione disulphonate. The iPSC single-cell suspensions were obtained by incubation in Gentle Dissociation Buffer (StemCell; Cat.No.: 07174) for 10 min at 37°C and filtering

through a Sterile Cell Strainer 70 μm nylon mesh filter. The growing single cell-derived colonies were subsequently monitored and selected by using direct fluorescence microscopy.

Characterization of genome-modifying events by long-range junction PCR

mCherry-positive iPSCs, wild-type myoblasts and DMD.B myoblasts generated after HR- or HMEJ-based genome editing strategies were sorted at ∼3 weeks post-transduction as whole populations or single cell-derived clones following the cell sorting and clonal expansion procedures described above. Genomic DNA from each sample was obtained with DNeasy Blood & Tissue kit (QIAGEN; Cat. No.: 69506) following the manufacturer's recommendations. Next, conventional and long-range junction PCR analyses were performed with GoTaq G2 DNA Polymerase (Promega; Cat. No.: M7801) and Platinum SuperFi II DNA Polymerase (ThermoFisher; Cat. No.:12361010), respectively. The PCR screening of the mCherry-positive cell populations and single cell-derived clones was performed using the PCR mixtures and cycling parameters indicated in Supplementary Table S5 and S6, respectively. Genomic DNA of HeLa cells exposed to AdVP.EGFP::DYS and AdVP.EGFP::DYS^{TS} alone, at an MOI of 8 TU ml^{-1}, or together with AdVP.eCas9^{4NLS}gRNA^{S1} at an MOI of 3×10^3 GC cell^{-1}, was retrieved instead at 28-days post-transduction. These samples were analysed with the PCR mixtures and cycling parameters indicated in Supplementary Tables S7 and S8, respectively.

Target DNA cleavage assays

Targeted DSB formation in cells transduced with AdVP.eCas9^{4NLS}gRNA^{S1} was assessed by using assays based on the mismatch sensing T7EI enzyme and amplicon sequencing. To this end, genomic DNA samples from mock-transduced and vector-transduced cells were retrieved at 3 days post-transduction using the DNeasy Blood & Tissue kit (QIAGEN; Cat. No.: 69506) following the manufacturer's recommendations. The *AAVS1* target site-specific PCR amplifications were performed using Phusion High-Fidelity DNA Polymerase (ThermoFisher; Cat. No.: F-530). The primer sequences, PCR mixture compositions and cycling parameters are specified in Supplementary Tables S9 and S10, respectively. The resulting amplicons were denatured and reannealed by applying the program listed in Supplementary Table S11. T7EI-based genotyping assays were done as follows. First, 10 μl of each PCR mixture was incubated in 15-μl reactions consisting of 1 × NEBuffer 2 (New England Biolabs; Cat. No.: B7002S) and 5 U of T7EI (New England Biolabs; Cat. No.: M0302). Next, after 17-min incubations at 37°C, the DNA samples were subjected to electrophoresis through 2% (w/v) agarose gels in 1 × Tris–acetate–EDTA (TAE) buffer. The resulting ethidium bromide-stained DNA species were then detected by using a Molecular Imager Gel-DocTM XR+ system (Bio-Rad) and the proportions of T7EI-digested products were determined by densitometry using Image Lab 6.0.1 software (Bio-Rad). Target DNA cleaving activities were determined by uploading Sanger sequencing traces corresponding to the target site-specific PCR products into the Inference of CRISPR Edits (ICE) tool https://ice.synthego.com/#/ (45).

Next-generation sequencing for off-target DNA cleavage analysis

Wild-type myoblasts were transduced with various MOI of AdVP.eCas9^{4NLS}gRNA^{S1} and cultures of the same cell type were co-transduced in parallel with comparable MOI of the second-generation *E1*- and *E2A*-deleted adenoviral vectors AdV$^{\Delta 2}$P.Cas9.F^{50} and AdV$^{\Delta 2}$U6.gRNA^{S1}.F^{50} (herein named AdV.Cas9 and AdV.gRNA^{S1}, respectively). AdV.Cas9 and AdV.gRNA^{S1} encode a wild-type Cas9 nuclease and the *AAVS1*-targeting gRNA gRNA^{S1}, respectively (46). At three days post-transduction, genomic DNA was isolated with the DNeasy Blood & Tissue kit reagents and protocol. To assess the specificity profiles of Cas9:gRNA^{S1} versus eCas9^{4NLS}:gRNA^{S1} complexes, a previously described amplicon deep sequencing analyses pipeline was used (47,48). In brief, the *AAVS1* target site and two off-target sites of Cas9:gRNA^{S1} complexes experimentally validated by orthogonal high-throughput genome-wide translocation sequencing (HTGTS), i.e. *CPNE5* and *BBOX1* (34), were first amplified with primers containing adapter tag overhangs using Phusion High-Fidelity Polymerase (Thermo Fisher Scientific; Cat. No.: #F-530L). The primer sequences, PCR mixture compositions and cycling parameters are specified in Supplementary Tables S12 and S13, respectively. The resulting amplicons were subsequently purified with AMPure XP beads (Beckman Coulter; Cat. No.: A63881) and subjected to PCR barcoding using Illumina tag-specific primer pairs with unique sequence combinations for demultiplexing and sample identification. The cycling parameters, primer sequences and PCR mixtures used for the preparation of barcoded amplicons are indicated in Supplementary Tables S13, S14 and S15, respectively. Next, the samples were further purified with AMPure XP beads and the concentrations of barcoded amplicons were determined by using the Qubit dsDNA HS assay kit (Thermo Fisher Scientific; Cat. No.: Q32854) and a Qubit2.0 fluorometer. Finally, purified amplicons were pooled in equal molar ratios and then subjected to Illumina MiSeq deep sequencing for retrieving 50 000 paired-end reads. Finally, after demultiplexing and adapter trimming of the paired-end MiSeq raw reads (R1 and R2 fastq files) with Cutadapt version 2.10 (49), alignment of amplicon sequences to reference sequences was carried out by using the CRISPResso2 software (50). The scripts applied in each CRISPResso2 analyses round are available as Supplementary Information.

Confocal immunofluorescence microscopy

Cultures of undifferentiated myoblasts and differentiated myotubes were analyzed through confocal immunofluorescence microscopy. This assay was also employed to detect the acquisition of differentiation markers (i.e. AFP,

FOXA2, α-SMA, CD31 and TUBB3) in germ line-specific cells derived from iPSCs. Cells cultured on glass coverslips were fixed with 4% paraformaldehyde (PFA) for 10 min. Next, after three washes with PBS, the cells were permeabilized in 0.5% (v/v) Triton X-100 in TBS (50 mM Tris-HCl pH 7.5, 100mM NaCl) at RT for 5 min and were then washed three times for 10 min with 0.1% Triton X-100 in TBS. Subsequently, the cells were exposed for 2 h to a blocking Antibody Diluting Solution (Abdil) consisting of 0.1% Triton X-100, 2% bovine serum albumin and 0.1% sodium azide in TBS. The specimens were then incubated overnight at 4°C with the proper primary antibodies diluted in blocking solution (Supplementary Table S16). After three 5-min washes with 0.1% Triton X-100 in TBS, the specimens were incubated with fluorochrome-conjugated secondary antibodies diluted in blocking solution for 1 h in the dark at RT (Supplementary Table S16). Finally, after three 10-min washes with 0.1% Triton X-100 in TBS, ProLong™ Gold Antifade Mounting reagent containing DAPI (ThermoFisher Scientific; Cat. No.: P36931) was used for mounting the specimens. Immunofluorescence microscopy images were acquired by using an upright Leica SP8 confocal microscope equipped with Leica hybrid detectors HyD or a 3DHISTECH Pannoramic 250 digital slide scanner for the detection and quantification of eCas9^{4NLS} expressing cells. The acquisition of differentiation markers (i.e. cTnI and sarcomeric α-actinin) by iPSC-derived cardiomyocytes was also assessed through immunofluorescence microscopy. The iPSC-derived cardiomyocytes were first dissociated by incubation for 10 min at 37°C in 5 × TrypLE Select (Thermo Fisher; Cat. No.: A1217701). The resulting cell suspensions were then seeded in wells of 96-well plates previously coated with Geltrex. After 4 to 6 days in culture medium, the cells were subjected to the same staining protocol described above except that (i) the cells were incubated overnight at 4°C in blocking solution, (ii) the cells were exposed to the appropriate primary antibody (Supplementary Table S16) for 2 h at RT and (iii) the nuclei were stained by incubation in Hoechst 33342 (Invitrogen; Cat. No.: H3570) diluted 1:1000 in PBS for 10 min at RT. Finally, microscopy images were analysed through the LAS X (Leica Microsystems), ImageJ (NIH, US National Institutes of Health) or CaseViewer (3DHISTECH) software packages whilst the cell image analysis software CellProfiler (51) at https://cellprofiler.org/#/, was employed for automated segmentation and quantification of eCas9^{4NLS}-positive nuclei.

Live-cell fluorescence microscopy

Reporter expression in HeLa cells, human myoblasts, iPSCs and iPSC-derived cardiomyocytes was monitored by direct fluorescence microscopy. mCherry- and EGFP-specific signals in HeLa cells, human myoblasts and iPSCs were detected by using an inverted DMi8 fluorescence microscope equipped with a DFC 450c camera. mCherry-specific signals in beating cardiomyocytes were recorded with a AF6000 LX system. The acquired images and videos were examined with the aid of LAS X (Leica Microsystems) and ImageJ software (NIH, US National Institutes of Health).

Western blotting

Unedited and vector-edited human myoblasts subjected to the differentiation conditions described previously were processed for western blot analysis as follows. After 4–6 days in differentiation medium, the myotube-containing cultures were lysed on ice for 30 min by incubation in 50 μl of RIPA buffer (ThermoFisher Scientific; Cat. No.: 89900) supplemented with a protease inhibitor cocktail (cOmplete Mini, Sigma-Aldrich; Cat. No.: 11836153001) and the resulting cell lysates were then passed through a 30-gauge syringe several times. Protein quantification was carried out by using the Pierce BCA Protein Assay Kit (ThermoFisher Scientific; Cat. No: 23225), following the manufacturer's instructions. Next, the indicated amounts of total protein were diluted in 4 × sample buffer (Bio-Rad; Cat. No.: 161–0791) and 20× reducing agent (Bio-Rad; Cat. No.: 161-0792), and were incubated at 95°C for 5 min. Protein samples and 15 μl of HiMark Prestained Protein Standard (ThermoFisher Scientific; Cat. No.: LC5699) were loaded in a 3–8% Criterion XT Tris-Acetate precast gel (Bio-Rad; Cat. No.: 3450130). The polyacrylamide gel was then placed in a Criterion Cell containing XT Tricine running buffer (Bio-Rad; Cat. No.: 1610790) and run for 30 min at 75 V (0.07 A) and for 1.5 h at 150 V (0.12 A). Subsequently, the resolved proteins were transferred to polyvinylidene difluoride (PVDF) membranes with the aid of a Trans-Blot Turbo Midi PVDF pack (Bio-Rad; Cat. No.: 1704157) and a Trans-Blot Turbo system (Bio-Rad) according to the manufacturer's recommendations for high-molecular-weight proteins (2.5 A, 25 V, 10 min). The PVDF membranes were then blocked for 2 h at room temperature in 5% non-fat dry milk (Campina Elk; Cat. No.: 112349) dissolved in TBS with 0.1% (v/v) Tween 20 (TBST). Next, the membranes were incubated overnight at 4°C with primary antibodies (Supplementary Table S17) diluted in 5% non-fat dry milk. After three 10-min washes in TBST, the membranes were incubated for 2 h at RT with the proper secondary antibodies (Supplementary Table S17) conjugated to horseradish peroxidase (IgG-HRP) diluted in 5% non-fat dry milk. Proteins were detected by using horseradish peroxidase substrate Pierce ECL2 (ThermoFisher Scientific; Cat. No.: 80196) following the manufacturer's specifications. iPSCs, instead, were lysed in Laemmli buffer consisting of 8.0% glycerol, 3% SDS and 200 mM Tris–HCl (pH 6.8) and subsequently incubated for 5 min at 100°C. Protein concentrations in cell lysates were assessed by using a DC™ protein assay kit (Bio-Rad; Cat. No.: 5000111) according to the manufacturer's recommendations. Proteins were separated by SDS-polyacrylamide gel electrophoresis (SDS-PAGE). Afterwards, the resolved proteins were transferred onto 45-μm PVDF membranes (Merck Millipore; Cat. No.: IPVH00010) that were subsequently blocked with 5% (w/v) non-fat dry milk dissolved in TBST at RT for 1 h. After the blocking step, the membranes were incubated overnight at 4°C with the proper primary antibody (Supplementary Table S17) diluted in TBST supplemented with 5% BSA. Next, the membranes were washed with TBST thrice and probed at RT for 2 h with the proper secondary antibody (Supplementary Table S17) diluted in TBST containing 1% (w/v) non-fat dry milk. Signal detection was per-

formed with the Clarity™ Western ECL Substrate (Bio-Rad; Cat. No.: 1705060). All images were acquired using Chemi-Doc Imaging System (Bio-Rad; Cat. No.: 17001402) and were analysed with the Image Lab 6.0.1 software (Bio-Rad).

Interphase FISH for DNA integration profile mapping

Cells were grown on glass coverslips to 80–100% confluency and were fixed with 4% PFA for 10 min followed by three washes with PBS for 5 minutes each. FISH was performed as described before (52) with some modifications. In brief, glass coverslips were pre-treated at 37°C for 10 min with 100 μg ml^{-1} RNase A (Roche; Cat. No.: 10154105103) in 2 × SSC (Sigma-Aldrich; Cat. No.: S0902) and were then incubated with 0.01% pepsin (Sigma-Aldrich; Cat. No.: P0525000) in 0.1 M HCl for 5 min at 37°C. After a 10-min fixation at room temperature with 1% (v/v) formaldehyde (Merck; Cat. No.: 1.03999.1000) in PBS (pH 7.4), the specimens were dehydrated by three 3-min incubations in ethanol at increasing concentrations, i.e. 70%, 90% and 100% and airdried. For interphase FISH, 25 ng of Cy3-dUTP nick translation labelled BAC probe (RP11-463M24) (Cy-dUTP Enzo Life Sciences; Cat. No: ENZ-42501) and 2.5 ng of Bio-11dUTP nick translation labelled transgene probe (Bio-11dUTP; Jena Biosciences; Cat. No.: NU-803-BIOX-S Nick translation) were used under a 12 mm round cover glass. The transgene probes covering the mCherry and full-length dystrophin expression cassettes, were obtained by enzymatic digestion and gel extraction of BE14_pAdVP.DYS.mCherry DNA using established procedures. After DNA denaturation at 80°C for 45 s, hybridizations were done for 18 h at 37°C in a humidified chamber. Unbound probes were removed first by washing with 0.1% Tween-20 (Promega; Cat. No.: PRH5152) in 2 × SSC, and then with 50% formamide (Merck; Cat. No.: 1.09684.1000) in 2× SSC (pH 7.0) at 44°C followed by incubation at 60°C in 0.1× SSC. Each washing step was done twice for 5 min. The biotin-labelled probe was detected by incubations in Streptavidin Alexa Fluor™ 488 Conjugate, diluted 1:250 (ThermoFisher; Cat. No.: S32354), followed by Biotinylated anti-Streptavidin diluted 1:100 (Jena Bioscienc; Cat. No.: BA-0500–5) and, finally, Streptavidin Alexa Fluor™ 488 Conjugate diluted 1:250 (ThermoFisher; Cat No: S32354). Each incubation took place at 37°C for 30 minutes and was followed by three washing steps in PBS for 5 min each. After dehydration by exposure to the above-mentioned increasing concentrations of ethanol, the specimens were air-dried and embedded in Citifluor AF1/DAPI (400 ng ml^{-1}) solution (Aurion; Cat. No.: E17970). Stained chromosomes were visualized with a Leica DMRA fluorescence microscope (Leica, Wetzlar, Germany) and images were captured with the aid of a CoolSnap HQ2 camera (Photometrics, Tucson, USA).

Molecular combing

Genome editing outcomes resulting from transducing human myoblasts with AdVPs designed for HR- or HMEJ-based gene targeting were assessed by using the molecular combing gene editing assay from Genomic Vision (Bagneux, France). Cells from control and AdVP-engineered cell lines were harvested and embedded in 1% low melting agarose plugs using the Genomic Vision FiberPrep® kit (Genomic Vision; Cat. No.: EXTR-001) at a concentration of 10 × 10^6 cells per plug. Subsequently, DNA extraction, combing, and immunostaining were performed according to the EasyComb procedure (Genomic Vision). Briefly, single long DNA molecules were extracted and stretched at a constant speed (∼2 kb μm^{-1}) onto the surface of vinyl silane-treated glass coverslips (CombiCoverslips) employing the automated Molecular Combing System (MCS) instrument (Genomic Vision). The linearity and density of the combed chromosome fibers were assessed by staining with the YOYO-1 dye to ensure precise and high-resolution measurements of hybridized DNA probes along the length of individually stretched DNA molecules (Supplementary Figure S1A). DNA probes corresponding to the EGFP::DYS fusion construct (recombinant probes) and to the *AAVS1* 'right' and 'left' homology arms (RHA and LHA probes, respectively) were isolated after enzymatic digestion and gel extraction of AO75_pHC.Ad.EGFP::DYS DNA using established procedures. All the other DNA probes covering the *AAVS1* target locus (i.e. 'right' and 'left' flank anchoring probes) were generated through long-range PCR amplification using the appropriate primer sets, reaction mixtures and cycling conditions (Supplementary Table S18 and S19). Next, FiberProbes® (Genomic Vision) were labelled and used as templates for FISH probe labelling by random priming. The correspondence between theoretical and experimental probe coverage patterns was validated by measuring probe hybridization lengths in control samples from unedited myoblasts (Supplementary Figure S1B). Finally, coverslips from control and experimental samples were hybridized to the various labelled probes and fluorescent signals were detected by using the FiberVision® automated scanner (Genomic Vision). Image analysis and signal measurements were performed by using the FiberStudio® software (Genomic Vision).

Statistical analysis

Statistical analyses were performed with the aid of GraphPad Prism software (version 8.0.1) on datasets derived from independent biological replicates or technical replicates as defined in the figure legends. Statistical significances were calculated with the tests specified also in the figure legends. *P*-values lower than 0.05 were considered statistically significant.

RESULTS

AdVPs achieve all-in-one delivery of optimized CRISPR-Cas9 complexes inducing robust and specific DNA cleavage

By lacking only a few viral ORFs, first- and second-generation adenoviral vectors do not permit exploiting the full DNA packaging capacity of adenoviral capsids, i.e. 36-kb (21,53). In addition, at high multiplicities of infection (MOI), 'leaky' expression from vector resident viral ORFs contributes to cytotoxic effects *in vitro* and immune responses *in vivo* (53). Therefore, in this study, we selected fully viral gene-deleted AdVPs (21,23–25) for investigating large-scale cell engineering strategies based

on the recruitment of homology-directed gene targeting processes. And, to broaden the target cell range, AdVPs were endowed with adenovirus type-50 fibers that, by engaging the ubiquitously expressed CD46 receptor (24,54), permit efficient transduction of otherwise refractory human myoblasts (55) and other coxsackievirus and adenovirus receptor (CAR)-negative cells with high therapeutic relevance. Hence, we first sought to generate a CD46-binding AdVP, namely AdVP.eCas9^{4NLS}gRNA^{S1}, for all-in-one transfer of optimized CRISPR-Cas9 components targeting *AAVS1* loci at 19q13.4-qter. We decided to target *AAVS1* owing to its common use as a safe harbor for transgene insertion and stable expression in a wide range of human cell types (56–58). AdVP.eCas9^{4NLS}gRNA^{S1} encodes a variant of the high-specificity eSpCas9(1.1) nuclease (59), called eCas9^{4NLS}, whose improved performance derives from having 2 extra nuclear localization signals (NLS) (60); and, an *AAVS1*-specific gRNA, named gRNA^{S1}, that harbors an optimized Cas9-binding scaffold (61) (Figure 1A). Importantly, AdVP.eCas9^{4NLS}gRNA^{S1} particles were produced at high titers (Supplementary Table S3) and contained structurally intact DNA with no evidence for rearranged or truncated species, as shown by restriction fragment length analysis (RFLA) (Figures 1B). To assess the functionality of AdVP.eCas9^{4NLS}gRNA^{S1} in delivering active eCas9^{4NLS}:gRNA^{S1} complexes into human cells, we transduced cervical carcinoma HeLa cells, wild-type human myoblasts and myoblasts derived from two separate DMD patients (hereinafter named DMD.A and DMD.B myoblasts) at MOI ranging from 1×10^3 to 50×10^3 genome copies per cell (GC cell^{-1}). As detected through T7 endonuclease I (T7EI)-based genotyping assays at three days post-transduction, eCas9^{4NLS}:gRNA^{S1} complexes readily led to DSB formation at *AAVS1* in all cell types tested (Figure 1C and Supplementary Figure S2). After applying AdVP.eCas9^{4NLS}gRNA^{S1} at 3×10^3, 5×10^3 and 10×10^3 GC cell^{-1}, targeted DNA cleaving activities ranging from 43% to 65%, 49% to 90%, 18% to 55% and 74% to 90% were measured by Sanger sequence deconvolution (45) in HeLa cells, DMD.A myoblasts, DMD.B myoblasts and wild-type myoblasts, respectively (Figure 1D). To assess the specificities of regular Cas9:gRNA^{S1} and optimized eCas9^{4NLS}:gRNA^{S1} complexes, wild-type myoblasts were co-transduced with adenovectors AdV.Cas9 and AdV.gRNA^{S1} (46) or were transduced with AdVP.eCas9^{4NLS}gRNA^{S1}, respectively. Consistent with earlier findings derived from orthogonal HTGTS assays in HEK293T cells (34), off-target DNA cleavage at *CPNE5* and *BBOX1* was readily detected by amplicon deep sequencing in human myoblasts exposed to Cas9:gRNA^{S1} complexes (Figures 1E and F). Crucially, independently of the AdVP dosages used, DNA cleavage at the same off-target sites was virtually undetected in human myoblasts that had been instead exposed to optimized eCas9^{4NLS}:gRNA^{S1} complexes (Figures 1E and F). Interestingly, supporting the view that Cas9 variants can lead to altered indel footprint profiles, at the highest vector doses applied, deletion size distributions induced by eCas9^{4NLS}:gRNA^{S1} were wider than those triggered by Cas9:gRNA^{S1} (Supplementary Figure S3).

Altogether, these data indicate that AdVP.eCas9^{4NLS}gRNA^{S1} is a reliable tool to efficiently and specifically induce targeted DSBs at the commonly used *AAVS1* safe harbor locus in human cells.

HMEJ donors yield higher CRISPR-Cas9-dependent genome editing frequencies than HR donors after AdVP delivery

Next, we sought to couple site-specific genomic DNA cleavage to AdVP delivery of donor DNA matched to *AAVS1* targeting through HR and HMEJ (Figure 2A). To this end, AdVP.EGFP::DYS and AdVP.EGFP::DYS^{TS}, encoding full-length dystrophin fused to the enhanced green fluorescent protein, were generated (Figure 2A). To test the versatility of AdVP-based genome editing strategies, AdV.DYS.mCherry and AdV.DYS.mCherry^{TS} were also assembled (Figure 2A). The former and latter vector have essentially the same structure as AdV.EGFP::DYS and AdV.EGFP::DYS^{TS}, respectively, except that, instead of a single expression unit, two independent expression units drive the synthesis of full-length dystrophin and reporter mCherry proteins (Figure 2A). Of notice, recombinant dystrophin and mCherry synthesis are under the control of late striated muscle-specific regulatory elements and a constitutively active promoter (i.e. CK8 and CAG, respectively) (Figure 2A). This bicistronic design guarantees therapeutic gene expression specifically in differentiated muscle cells and offers the possibility for isolating stem/progenitor cells with myogenic capacity by constitutive expression of a clinically applicable selection marker, e.g. truncated nerve growth factor receptor (62). AdVP.EGFP::DYS and AdVP.DYS.mCherry have their expression cassettes surrounded by 5.1 kb of DNA sequences identical to the genomic DNA flanking the gRNA^{S1} target site (homology arms) to favor DSB-induced transgene insertion through HR. In order to engage not only HR but also HMEJ processes, AdVP.EGFP::DYS^{TS} and AdVP.DYS.mCherry^{TS} contain the gRNA^{S1} target site at the outward extremities of the 5.1 kb homology arms. This arrangement assures eCas9^{4NLS}:gRNA^{S1}-mediated donor DNA release from AdVP genomes, to facilitate its targeted insertion through HMEJ.

Like for AdVP.eCas9^{4NLS}gRNA^{S1}, the integrity of vector genomes in all AdVP donors was confirmed by RFLA of DNA isolated from purified vector particles (Supplementary Figure S4). Physical particle titers were determined by quantification of packaged vector genome copies (Supplementary Table S3), while functional particle titers of purified preparations of AdVP.EGFP::DYS, AdVP.EGFP::DYS^{TS}, AdVP.DYS.mCherry and AdVP.DYS.mCherry^{TS} were in turn determined by end-point titration assays on HeLa cells followed by quantification of transduced cells by reporter-directed flow cytometry. The functional particle titers of AdVP.EGFP::DYS, AdVP.EGFP::DYS^{TS}, AdVP.DYS.mCherry and AdVP.DYS.mCherry^{TS} were, respectively, 5.23×10^8 HeLa-transducing units per ml (TU ml^{-1}), 3.92×10^8 TU ml^{-1}, 7.38×10^{10} TU ml^{-1} and 7.42×10^{10} TU ml^{-1} (Supplementary Table S3).

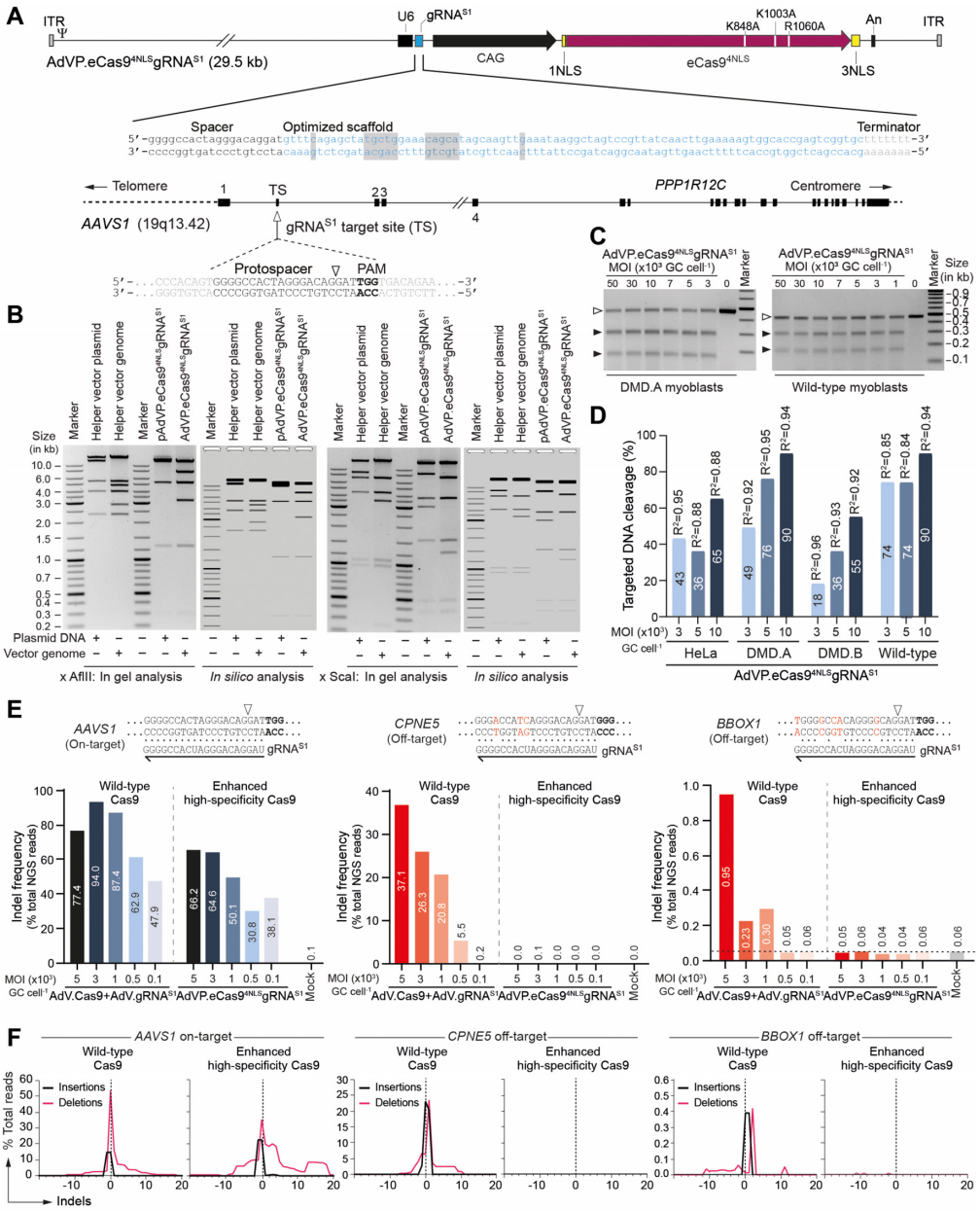

Figure 1. Characterization and testing of AdVP for all-in-one delivery of optimized *AAVS1*-targeting RGN complexes. (**A**) Schematics of AdVP genome encoding eCas9^{4NLS}:gRNA^{S1} complexes and *AAVS1* target site. Enhanced high-specificity eCas9^{4NLS} nuclease and optimized gRNA^{S1} synthesis are driven by hybrid CAG regulatory sequences and the human *U6* gene promoter, respectively. The point mutations conferring enhanced specificity to the optimized eCas^{4NLS} nuclease are specified. The point mutations and insertions in the gRNA scaffold coding sequence that maximize the expression of full-length RNA molecules with a stabilizing extended stem-loop are shaded. NLS, nuclear localization signal (NLS); ITR and Ψ, adenoviral inverted terminal repeats and packaging signal *cis*-acting elements for vector DNA replication and encapsidation, respectively. The *AAVS1* target site locates in the first intron of *PPP1R12C* (19q13.42). The gRNA^{S1} protospacer and protospacer adjacent motif (PAM) sequences are highlighted. Open arrowheads indicate the DNA cleavage position. (**B**) Assessing AdVP.eCas9^{4NLS}gRNA^{S1} DNA integrity. Restriction fragment length analysis (RFLA) of vector DNA isolated from purified AdVP.eCas9^{4NLS}gRNA^{S1} particles. *In-silico* and in-gel RFLA analyses are presented. Parental circular plasmid pAdVP.eCas9^{4NLS}gRNA^{S1} and helper vector DNA used to assemble AdVP.eCas9^{4NLS}gRNA^{S1} particles served as molecular weight references. (**C**) Probing AdVP.eCas9^{4NLS}gRNA^{S1} functionality. The indicated target cells were exposed to different amounts of AdVP.eCas9^{4NLS}gRNA^{S1} and site-specific DNA cleavage was assessed at 3 days post-transduction through the detection of DSB-derived indels using the mismatch-sensing T7EI enzyme. Solid and open arrowheads point to DNA species derived from T7EI-digested and undigested amplicons, respectively. MOI, multiplicity of infection in genome copies per cell (GC cell^{-1}); Marker, GeneRuler DNA Ladder Mix. (**D**) Quantification of target DNA cleavage. The eCas9^{4NLS}:gRNA^{S1} activities were measured by deconvolution of Sanger sequence traces corresponding to *AAVS*1-specific amplicons derived from the indicated target cells exposed to three doses of AdVP.eCas9^{4NLS}gRNA^{S1}. (**E**) Assessing the specificity of Cas9:gRNA^{S1} versus eCas9^{4NLS}:gRNA^{S1} complexes. Wild-type myoblasts were exposed to AdVP.eCas9^{4NLS}gRNA^{S1} or to AdVP.Cas9 and AdVP.gRNA^{S1} at the indicated total MOI. DNA cleaving activities at the *AAVS1* target site and at two validated off-target sites (i.e. *CPNE5* and *BBOX1*) were quantified by amplicon deep sequencing of DSB-derived indels at three days post-transduction (~50,000 paired-end reads per sample). Nucleotide mismatch positions between gRNA^{S1} spacer and off-target *CPNE5* and *BBOX1* sequences are highlighted in red. (**F**) Characterization of nuclease-induced indel footprints by amplicon deep sequencing. Wild-type myoblasts were exposed to AdVP.eCas9^{4NLS}gRNA^{S1} or to AdVP.Cas9 and AdVP.gRNA^{S1} at an MOI of 5×10^3 GC cell^{-1} each. The types and distributions of indels detected within *AAVS1*, *CPNE5* and *BBOX1* are plotted.

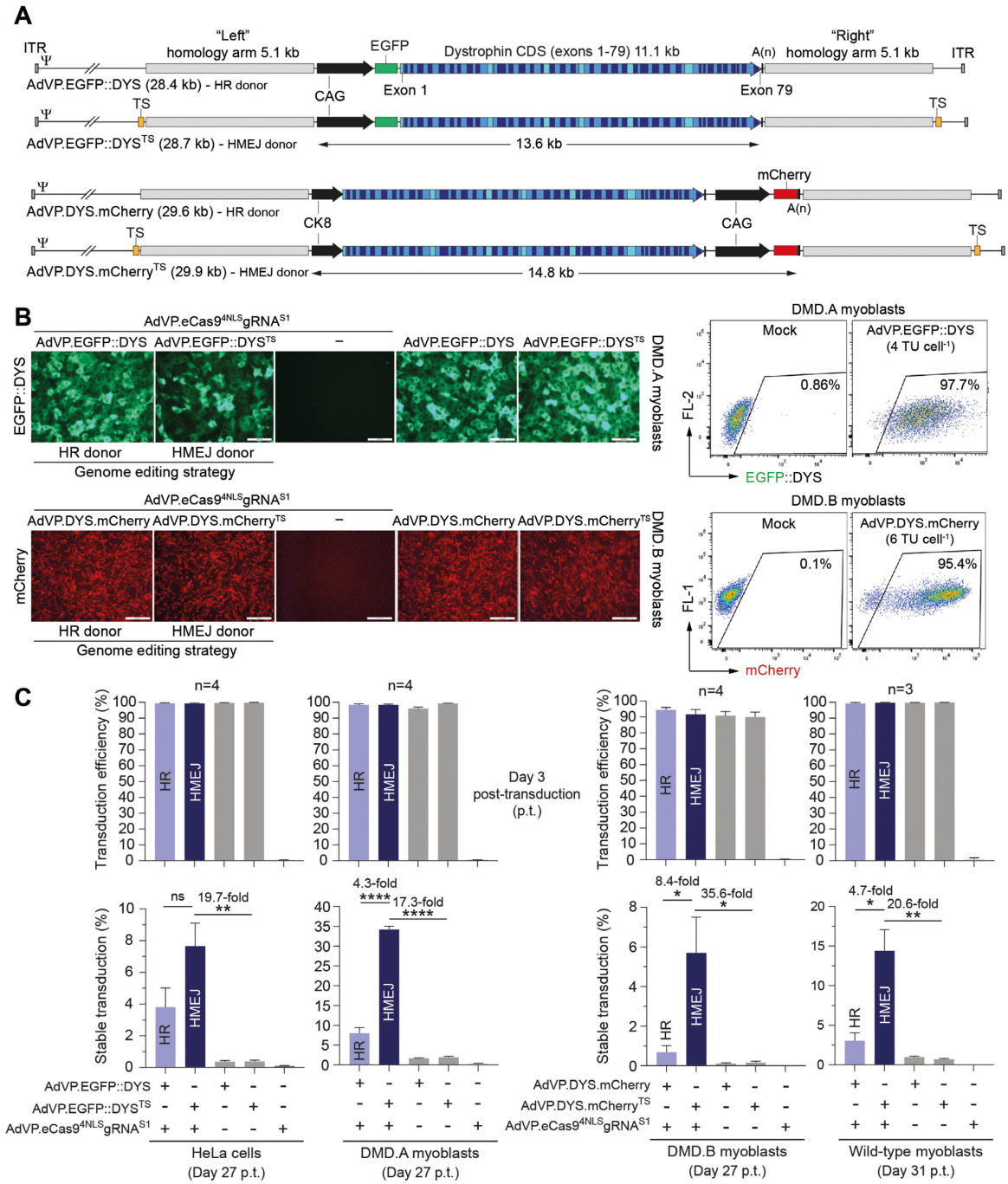

Figure 2. Assembly and testing of AdVP donors designed for homology-directed genome editing. (**A**) Schematics of AdVP donor structures. In AdVP.EGFP::DYS and AdVP.EGFP::DYS^{TS}, the CAG promoter drives the synthesis of a fusion product between EGFP and the human full-length dystrophin (EGFP::DYS). In AdVP.DYS.mCherry and AdVP.DYS.mCherry^{TS}, striated muscle-specific CK8 and constitutive CAG promoters drive the synthesis of full-length dystrophin (DYS) and the mCherry live-cell reporter, respectively. The recombinant DNA in the various vectors is flanked by sequences homologous to the human *AAVS1* safe harbor locus for testing homology-directed gene targeting upon site-specific DSB formation. AdVP.EGFP::DYS^{TS} and AdVP.DYS.mCherry^{TS} differ from AdVP.EGFP::DYS and AdVP.DYS.mCherry in that they have their targeting modules flanked by the gRNA^{S1} target site (TS). This arrangement guarantees targeted DSB formation at endogenous and exogenous DNA sequences for generating donor substrates amenable to HMEJ. ITR and Ψ, inverted terminal repeats and packaging elements, respectively. (**B**) Testing AdVP donors in human myoblasts. Transduction efficiencies were determined by reporter-directed fluorescence microscopy and flow cytometry at three days post-transduction (left and right panels, respectively). Representative micrographs and dot plots of DMD myoblasts from two different sources (A and B) transduced with the indicated AdVP donors are shown. Controls consisted of cells transduced solely with each AdVP donor or only with AdVP.eCas9^{4NLS}gRNA^{S1}. (**C**) Assessing stable transduction frequencies upon AdPV delivery of HR and HMEJ donors. Transduction efficiencies (top graphs) and stable transduction levels (bottom graphs) reached in the indicated cell types were determined by reporter-directed flow cytometry at three days and over three weeks post-transduction, respectively. The AdVP transduction conditions used in these experiments are listed in Supplementary Table S20. Data are presented as mean ± SEM of either four or three independent biological replicates. Significant differences between the indicated datasets were determined by Student's *t*-tests; $^{****}P < 0.0001$, $^{**}P < 0.01$; $^{*}P < 0.05$. $P > 0.05$ was considered non-significant (ns).

Importantly, transduction of human myoblasts with these AdVP donors resulted in transgene expression in most of the target cells independently of their individual origins (Figure 2B).

Next, to assess stable transgene expression levels, human cells were initially transduced with AdVP.eCas9^{4NLS}gRNA^{S1} together with AdVP donors whose genomes are insensitive (i.e. AdVP.EGFP::DYS and AdVP.DYS.mCherry) or susceptible (i.e. AdVP.EGFP::DYS^{TS} and AdVP.DYS.mCherry^{TS}) to site-specific DNA cleavage. Controls consisted of cells transduced with each AdVP individually. Dual color fluorescence microscopy analyses confirmed the capacity of AdVPs delivering separately nuclease and donor DNA constructs to co-transduce target cells (Supplementary Figure S5), and western blot analysis established transient nuclease expression in dividing cell populations, as shown by the rapid decline in nuclease amounts after a peak at 2 days post-transduction (Supplementary Figure S6).

At three days post-transduction, over 90% of target cells exposed to AdVP donors expressed reporter proteins, as determined through flow cytometry (Figure 2C top graphs). The transduced cell populations were then sub-cultured for >3 weeks to remove episomal vector DNA (Supplementary Figure S7) and, during this period, were monitored through reporter-directed flow cytometry (Supplementary Figure S8). This analysis revealed a clear CRISPR-Cas9-dependent increase in stable transduction levels (Figure 2C bottom graphs and Supplementary Figure S8). In addition, although the frequencies of stably transduced cells varied in a target cell-dependent manner, AdVP donors delivering templates susceptible to HMEJ (i.e. AdVP.EGFP::DYS^{TS} and AdVP.DYS.mCherry^{TS}) invariably led to higher stable transduction levels than those transferring templates strictly susceptible to HR (i.e. AdVP.EGFP::DYS and AdVP.DYS.mCherry) (Figure 2C, bottom graphs and Supplementary Figure S8). These flow cytometry datasets were consistent with those obtained through qPCR tracing of HR and HMEJ donor DNA upon AdVP transductions (Supplementary Figure S7). Finally, junction PCR assays revealed that the clear CRISPR-Cas9-dependent increase in stable transduction levels (Figure 2C bottom graphs, and Supplementary Figures S7 and S8), was accompanied by the detection of targeted chromosomal insertion of HR and HMEJ donor DNA in cells exposed to eCas9^{4NLS}:gRNA^{S1} complexes (Figure 3).

Long-term constitutive expression of full-length dystrophin was confirmed through confocal microscopy and western blot analyses of genetically corrected DMD muscle cell populations prior to, and after, myogenic differentiation (Figures 4A, B and Supplementary Figure S9). Co-detection in myotubes of the late skeletal muscle-specific marker sarcomeric α-actinin and full-length dystrophin by confocal microscopy ascertained the differentiation capacity of DMD muscle progenitor cells endowed with constitutive and CK8-regulated expression units (Figure 4C and Supplementary Figure S9, respectively). Taken together, these data establish that HMEJ donors delivered in the context of AdVP genomes yield higher CRISPR-Cas9-mediated genetic correction than their HR counterparts in muscle progenitor cells and that the AdVP platform can be tailored for the permanent complementation of DMD-causing mutations in patient-derived muscle cells.

Large-scale engineering of iPSCs through AdVP-based HR and HMEJ genome editing

Combining genome editing and iPSC technologies is appealing for establishing 'disease-in-a-dish' models, building robust multi-component synthetic gene circuits, and investigating autologous cell therapies (63–65). In this context, the use of AdVPs as sources of donor DNA has been hitherto mostly explored for mutation-specific gene correction through spontaneous HR (24). Despite the association of large homology tracts to short exogenous sequences, these programmable nuclease-independent AdVP genome editing approaches yield low frequencies of engineered iPSCs (i.e. 10^{-6}–10^{-5}), as generally determined by the ratios between drug-resistant to transduced-cell numbers. Moreover, the performance of HMEJ donors in iPSCs and its comparison with that of conventional HR donors requires investigation.

Therefore, we next set out to test AdVP-based HR and HMEJ strategies for large-scale engineering of iPSCs and, to this end, DMD patient-derived iPSCs (DMD iPSCs) were transduced with AdVP.eCas9^{4NLS}gRNA^{S1} in combination with AdV.DYS.mCherry or AdV.DYS.mCherry^{TS}. As controls, DMD iPSCs were exposed to each vector separately. Transduction levels of ∼80% were measured through mCherry-directed flow cytometry at four days post-transduction (Figure 5A, top graph). Subsequent subculturing followed by mCherry-directed flow cytometry at 19 days post-transduction revealed a CRISPR-Cas9-dependent increase in the frequencies of stably expressing DMD iPSCs (Figure 5A, bottom graph). These frequencies (∼0.1%) were substantially lower than those detected in human myoblasts exposed to the same vector combinations (Figure 2C, bottom graphs), which in turn correlated with the detection of lower amounts of targeted DSB-derived indels in DMD iPSCs (Supplementary Figure S10). Moreover, differently from the transduction experiments in HeLa cells and human myoblasts (Figure 2C), in DMD iPSCs, HR and HMEJ donors performed comparably (Figure 5A bottom graph). Notwithstanding, DMD iPSCs genetically modified through the AdVP-based HR and HMEJ strategies (Figure 5B), were confirmed to have undergone homology-directed chromosomal insertion of the exogenous DNA, as demonstrated by junction PCR analysis on bulk populations and randomly isolated cell clones (Figure 5C and Supplementary Figure S11). Moreover, the resulting genome-edited iPSCs remained pluripotent as shown by their ability to differentiate along the three embryonic germ layers (Figure 5D). Finally, further supporting their self-renewal and multilineage potential, genome-edited iPSCs could differentiate into cardiomyocyte-like cells, as established by the detection of the striated and cardiac muscle markers sarcomeric α-actinin and cardiac troponin I (cTnI), respectively (Supplementary Figre S12), as well as by the acquisition of a spontaneously beating phenotype (Supplementary Data File 1).

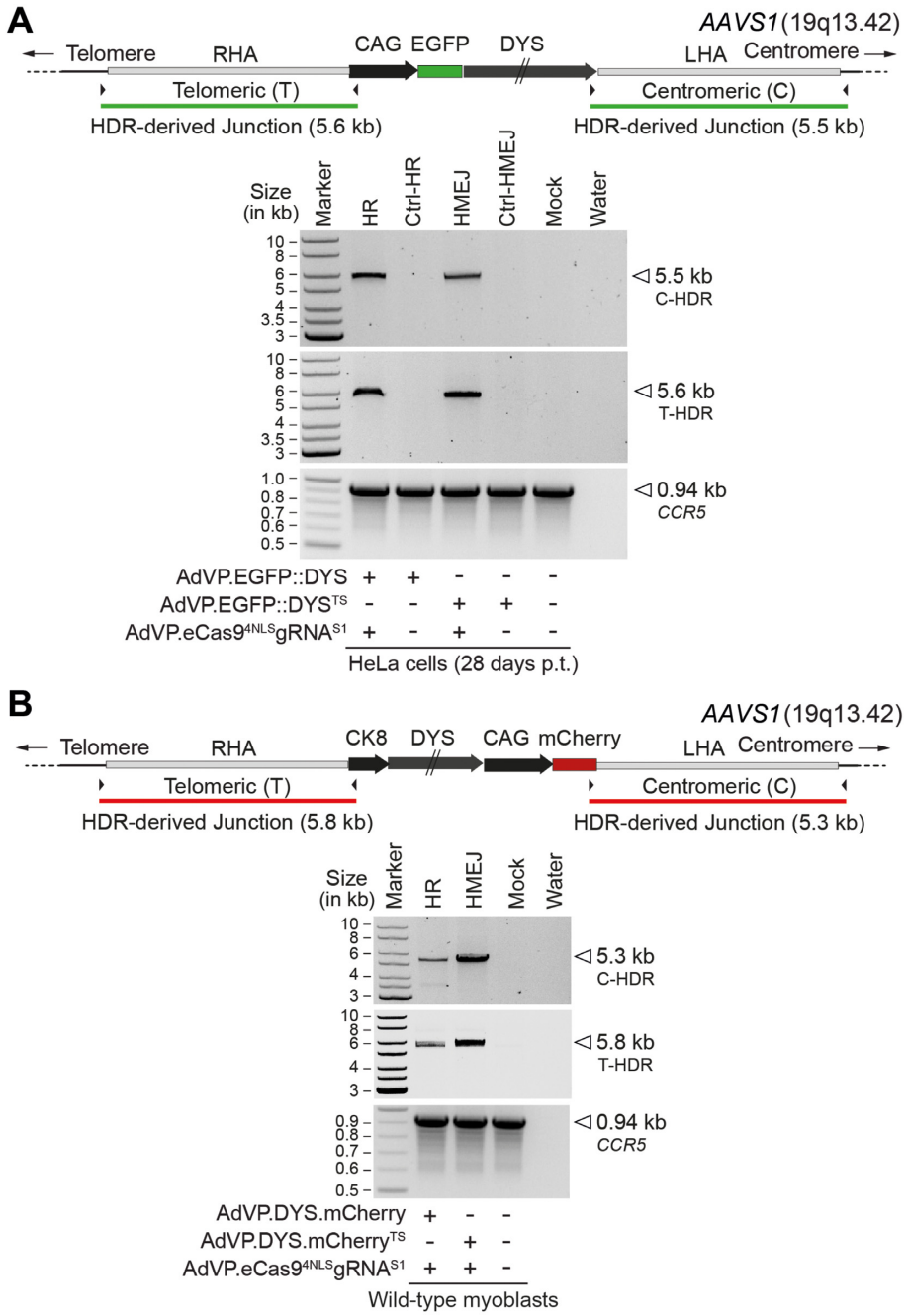

Figure 3. Targeted chromosomal DNA integration in human cells upon AdVP transduction. (**A**) AdVP-based genome editing in HeLa cells. Long-range junction PCR detection of *AAVS1*-targeted insertions in unselected HeLa cell populations exposed to the indicated donor and nuclease constructs at 8 TU cell^{-1} and 3 × 10^3 GC cell^{-1}, respectively. (**B**) AdVP-based genome editing in human myoblasts. Long-range junction PCR detection of *AAVS1*-targeted insertions in human myoblasts genetically modified through co-transduction with the indicated donor and nuclease constructs at 10^2 TU cell^{-1} and 5 × 10^3 GC cell^{-1}, respectively. Amplicons diagnostic for telomeric-sided transgenic-*AAVS1* junctions (T-HDR) and centromeric-sided transgenic-*AAVS1* junctions (C-HDR) junctions are depicted. *CCR5* served as an internal control template. Marker, GeneRuler DNA Ladder Mix. RHA and LHA, 'right' and 'left' homology arms, respectively.

TP53 downregulation facilitates HMEJ-based genome editing in iPSCs

It is well-known that stem cells are particularly sensitive to DSBs and that inhibiting the p53-dependent DNA damage response can increase the frequencies of stem cells edited through CRISPR-Cas9-induced NHEJ or ectopic HR (66,67). However, the impact of p53 on HMEJ-mediated genome editing strategies, in which cells are exposed to chromosomal and episomal DSBs, requires investigation. To this end, we started by generating independent iPSC lines (i.e. DMD iPSCs and wild-type iPSCs) containing low and normal amounts of p53. This p53 modulation was accomplished via lentiviral vector expression

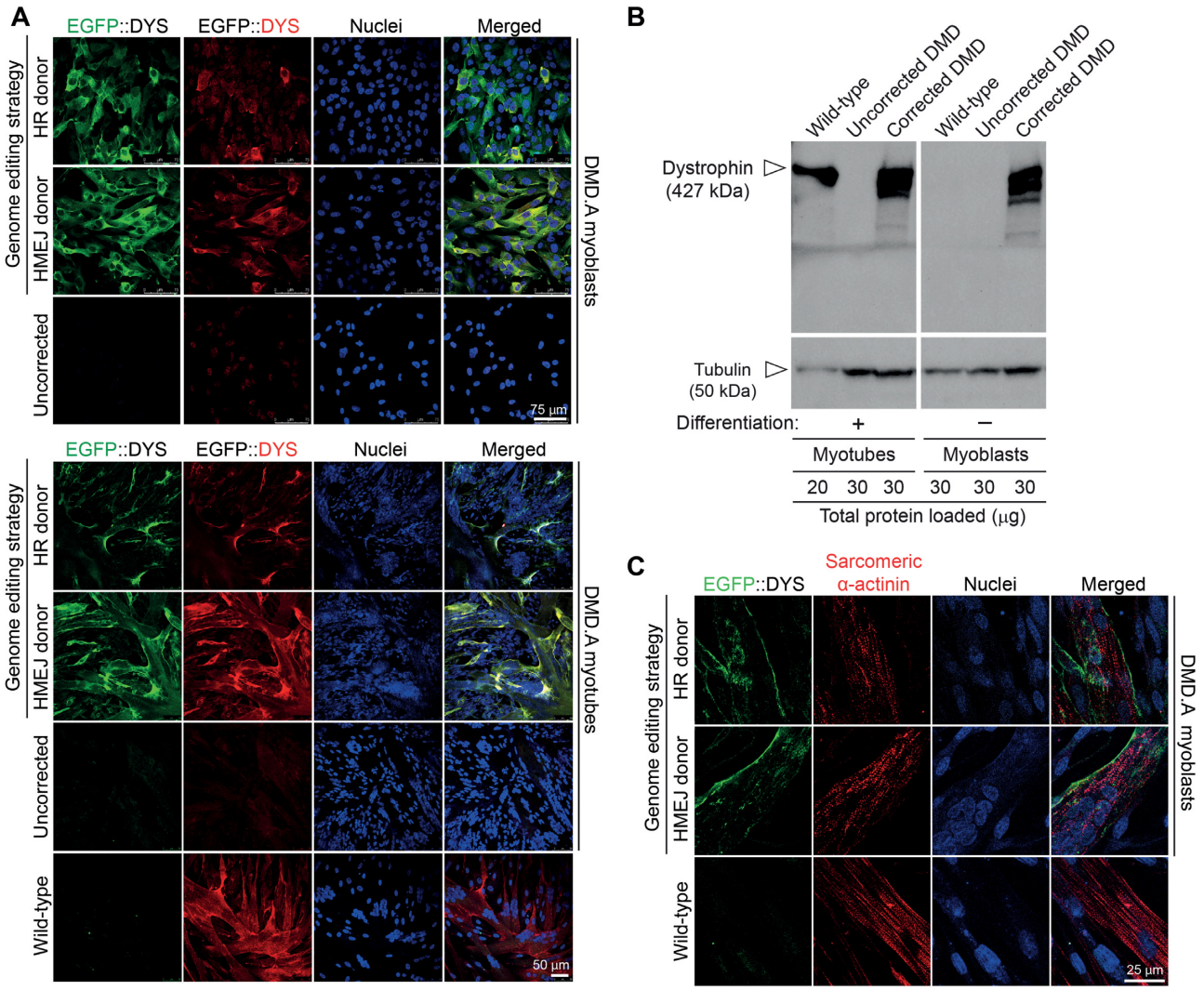

Figure 4. Rescue of full-length dystrophin synthesis in AdVP-corrected DMD muscle cells. (**A**) Detection of dystrophin by fluorescence microscopy. Fluorescence microscopy analyses on DMD patient-derived muscle cells stably expressing EGFP::DYS after AdVP delivery of eCas9^{4NLS}:gRNA^{S1} together with HR or HMEJ donor templates. These analyses were done before and after muscle cell differentiation (top and bottom panels, respectively). Uncorrected DMD muscle cells and healthy donor-derived muscle cells served as negative and positive controls, respectively. (**B**) Detection of dystrophin by western blot analysis. Western blotting was performed on uncorrected and corrected DMD muscle cells after (+) and before (–) myogenic differentiation. Differentiated wild-type muscle cells served as a reference for endogenous full-length dystrophin expression. Detection of tubulin provided for protein loading controls. (**C**) Detection of sarcomeric α-actinin by immunofluorescence microscopy. Assessing the differentiation capacity of AdVP-edited DMD myoblasts by co-detection of fluorescence signals specific for EGFP::DYS and the late muscle cell marker sarcomeric α-actinin. Nuclei were labelled with the DNA dye DAPI.

of short-hairpin RNAs targeting human *TP53* (shp53) and bacterial *LacZ* (shLacZ) transcripts, respectively. A robust shp53-dependent *TP53* knockdown, concomitant with significant downregulation of three canonical p53-responsive genes (i.e. *p21*, *FAS* and *PUMA*), was established through RT-qPCR analyses (Figure 6A). This strict shp53-mediated gene silencing was corroborated at the protein level by western blot analysis (Supplementary Figure S13).

Next, the various iPSC lines were co-transduced with AdVP.eCas9^{4NLS}gRNA^{S1} and AdV.DYS.mCherry or with AdVP.eCas9^{4NLS}gRNA^{S1} and AdV.DYS.mCherry^{TS} and, once again, controls consisted of cells transduced with each AdVP individually. Transductions with AdVP donors resulted in transgene expression in the vast majority of DMD iPSCs and wild-type iPSCs as monitored by direct fluorescence microscopy (Figure 6B) and quantified by flow cytometry at 3 days post-transduction (Figure 6C, top graphs). Moreover, iPSCs with regular and reduced amounts of p53 were transduced similarly well (Figure 6C, top graphs). After over 2.5 weeks of subculturing, mCherry-directed flow cytometry revealed that the CRISPR-Cas9-dependent increase in stable transduction levels was, on a per experimental setting basis, roughly one order of magnitude higher in wild-type than in DMD iPSCs (Figure 6C, bottom graphs). In itself, this result underscores the notion that the susceptibility of different iPSC lines to genome editing interventions can vary greatly. Interestingly, p53 knockdown led to significant and

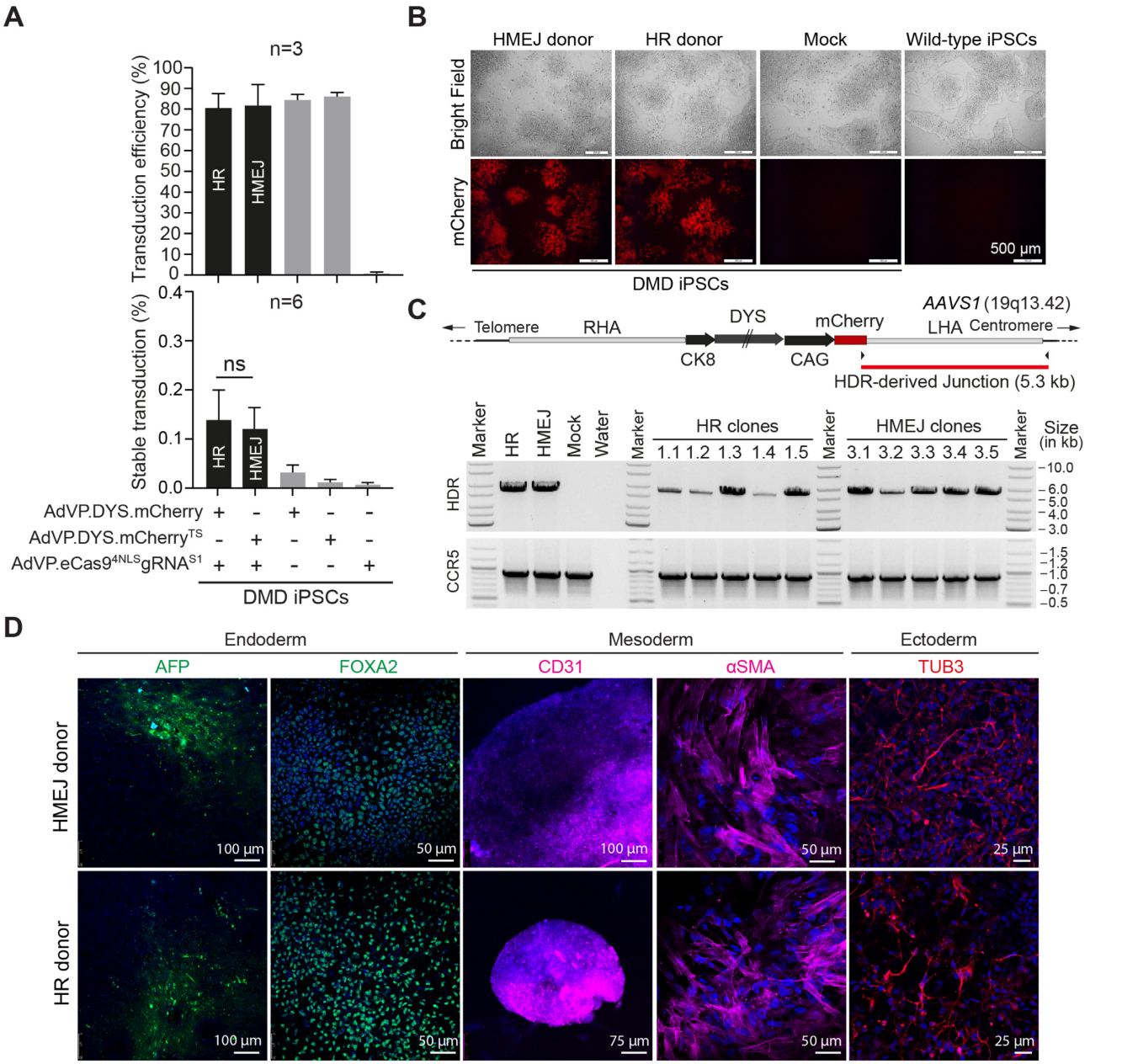

Figure 5. Testing AdVP-based HR and HMEJ genome editing strategies in iPSCs. (**A**) Testing AdVP donors encoding full-length dystrophin in DMD patient-derived iPSCs. Transduction efficiencies (top graph) and stable transduction levels (bottom graph) in iPSCs with a deletion of *DMD* exons 45 through 50 (DMD iPSCs), were determined by mCherry-directed flow cytometry at 4 and 19 days, respectively, after transduction with the indicated AdVPs. Bars and error bars correspond to mean ± SEM, respectively. Student's *t*-test showed non-significant (ns) differences between the indicated datasets ($n = 6$ biological replicates; $P > 0.05$). (**B**) Stably transduced DMD iPSCs. Representative micrographs of mCherry-sorted DMD iPSCs initially transduced with AdVP.eCas9^{4NLS}gRNA^{S1} at 5×10^3 GC cell^{-1} together with AdVP.DYS.mCherry (HR donor) or with AdVP.DYS.mCherry^{TS} (HMEJ donor) at 10^2 TU cell^{-1} each. Controls consisted of wild-type iPSCs and parental mock-transduced DMD iPSCs. (**C**) Establishing targeted chromosomal integrations. Long-range junction PCR analysis on DMD iPSC populations genetically modified through AdVP-based HR or HMEJ genome editing strategies and randomly isolated iPSC clone derivatives. Amplicons diagnostic for centromere-sided transgenic-*AAVS1* junctions are depicted. *CCR5* served as an internal control template. Marker, GeneRuler DNA Ladder Mix. (**D**) Characterization of AdVP-edited DMD iPSCs. The pluripotency of genome-edited DMD iPSCs was ascertained by spontaneous differentiation and immunofluorescence detection of markers covering the three embryonic germ layers. Nuclei were identified by DAPI staining.

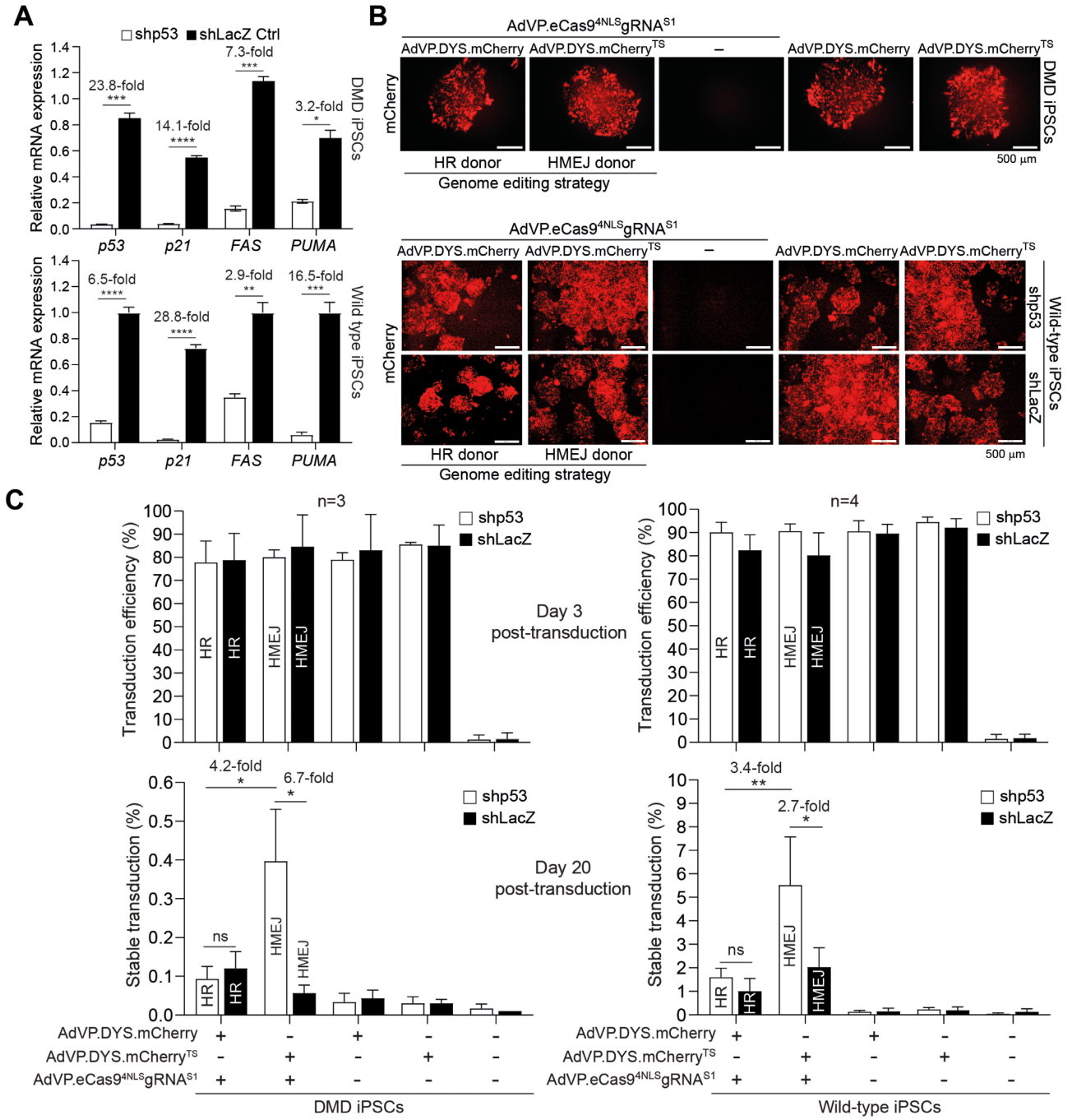

Figure 6. Effect of p53 knockdown on AdVP-based HR and HMEJ genome editing strategies in iPSCs. (**A**) Functional p53 knockdown in human iPSCs. RT-qPCR analysis of the indicated p53-responsive genes in dystrophin-defective and wild-type iPSCs stably expressing shRNAs targeting p53 (shp53) or control LacZ transcripts (shLacZ). Data are plotted as mean ± SEM of three technical replicates. Significances between the indicated datasets were calculated with Student's *t*-tests; $****P < 0.0001$, $***P < 0.001$, $**P < 0.01$, $*P < 0.05$. (**B**) Probing AdVP transduction efficiencies in normal and p53 knockdown iPSCs. Direct fluorescent microscopy analysis on the indicated iPSCs at 2 days after transduction with AdVP.eCas9^{4NLS}gRNA^{S1} at 5×10^3 GC cell^{-1} together with AdVP.DYS.mCherry (HR donor) or with AdVP.DYS.mCherry^{TS} (HMEJ donor) at 10^2 TU cell^{-1} each. Controls consisted of cells individually transduced with AdVP donors or AdVP.eCas9^{4NLS}gRNA^{S1}. (**C**) Testing AdVP-based HR and HMEJ genome editing strategies in normal and p53 knockdown iPSCs. Transduction efficiencies (top graph) and stable transduction levels (bottom graph) in wild-type and DMD iPSCs expressing shp53 or control shLacZ were assessed by mCherry-directed flow cytometry at 3 and 20 days post-transduction, respectively. AdVP.eCas9^{4NLS}gRNA^{S1} and AdVP donors were applied at 5×10^3 GC cell^{-1} and 10^2 TU cell^{-1}, respectively. Data are presented as mean ± SEM of at least three biological replicates. Significances between the indicated datasets were calculated with Student's *t*-tests. $**P < 0.01$, $*P < 0.05$. $P > 0.05$ was considered non-significant (ns).

non-significant enhancing effects on the performance of the HMEJ- and HR-based genome editing strategies, respectively. Together, these data indicate that the observed blunted performance of HMEJ-based genome editing in iPSCs can be rescued to a significant degree via interfering with p53 function (Figure 6C, bottom graphs).

Finally, we performed COBRA-FISH molecular karyotyping to probe the genetic stability of iPSCs with regular or reduced p53 levels and subjected to HR- or HMEJ-based genome editing upon AdVP transduction. Regardless of the iPSC population tested, at the level of COBRA-FISH karyotyping resolution, neither numerical alterations (monosomy or trisomy) nor structural alterations (i.e. translocations, insertions, or deletions) were detected and a prevalence of cells with 2N was observed (Supplementary Figure S14A). DNA content analysis of actively cycling iPSC populations using propidium iodide-directed flow cytometry confirmed the prevalence of 2N followed by 4N cell fractions (Supplementary Figure S14B). Besides DNA replication, the acquisition of a complete 4N ploidy number, or higher, can occur through endoreduplication whereby an extra round or more of DNA synthesis is not followed by cytokinesis yielding endopolyploid cells. Nonetheless, clearly, future p53 inhibiting agents selected for fostering HMEJ-based genome editing should act in a strictly transient fashion due to the notorious role of *TP53* as a tumor-suppressor gene supporting genomic stability.

Characterization of large-scale genomic edits in human myoblasts enabled with AdVPs

Junction PCR analysis established homology-directed chromosomal insertion of exogenous DNA through AdVP-based HR and HMEJ genome editing in HeLa cells (Figure 3A), human myoblasts (Figure 3B) and iPSCs (Figure 5C and Supplementary Figure S11). Additionally, next to targeted chromosomal insertions, interphase FISH revealed the presence of off-target insertions in wild-type and DMD.B myoblasts (Supplementary Figure S15). To complement these data, we next applied molecular combing to characterize genome editing events underlying stable expression of full-length, hence fully functional, dystrophin in human muscle cells. AdVP delivery of CRISPR-Cas9 nucleases and donor DNA constructs designed to favor HR and HMEJ resulted in 8.0 ± 1.4% and 34.1 ± 0.9% of EGFP::DYS-positive DMD.A myoblasts, respectively (Figure 2C bottom graphs). These unselected cell populations served as source material for the molecular combing analysis with mock-transduced cell populations acting as controls. Molecular combing analysis consists of fluorescence-based detection of probe hybridization to recombinant and human sequences in stretched single chromosome fibers (Figure 7A and Supplementary Figure S1). The probe coverage measurements in individual chromosome fibers from mock-transduced cultures (Supplementary Figure S1B) and in transgene-negative chromosome fibers from AdVP-transduced cultures (Figure 7B left panels), generally coincided with the DNA lengths expected for unmodified *AAVS1* alleles. Importantly, the same measurements in transgene-positive fibers mostly corresponded to precisely targeted *AAVS1* alleles (Figure 7B right panels and Supplementary Figure S16). Indeed, this analysis revealed that in the cell fractions genetically modified with HR and HMEJ donor sequences, CRISPR-Cas9-induced *AAVS1* integration occurred at frequencies of 71.5% and 93.5%, respectively (Figure 7C). Amongst the targeted HR and HMEJ donor DNA insertions, 62.3% and 73.3% were precise, corresponding to 87.1% and 78.4% of the total targeted events, respectively (Figure 7C). In addition to these precise single-copy targeted DNA insertions, genome-edited cell populations also contained lower fractions of multiple-copy targeted DNA insertions (Figure 7C and Supplementary Figure S16). Moreover, albeit at a low frequency, site-specific chromosomal insertions consistent with direct end-to-end ligation of excised HMEJ donor DNA to *AAVS1*, were detected in human myoblasts initially co-transduced with AdVP.eCas9^{4NLS}gRNA^{S1} and AdVP.EGFP::DYS^{TS},i.e., homology-independent recombinant DNA insertions (Figure 7C right panel and Supplementary Figure S16). As expected, these homology-independent genome editing events, presumably resulting from NHEJ-mediated 'capture' of donor DNA at site-specific *AAVS1* breaks, were not detected in human myoblasts initially co-transduced with AdVP.eCas9^{4NLS}gRNA^{S1} and AdVP.EGFP::DYS (Figure 7C, left panel). Importantly, regardless of the targeted genome-editing precision, all probe coverage measurements were consistent with the integration of complete dystrophin expression units (Figure 7C). Finally, off-target donor DNA insertions and *AAVS1* DNA rearrangements, the latter possibly caused by unbalanced translocation elicited by CRISPR-Cas9-induced DSBs, were also observed in myoblast populations subjected to both genome editing strategies (Figure 7D and Supplementary Figure S16). In conclusion, molecular combing analysis confirmed that genetic modification through AdVP-based HR and HMEJ genome editing strategies mostly involves exogenous DNA integration at *AAVS1* with most of these events corresponding to precise chromosomal DNA insertions.

DISCUSSION

In this study, we report that AdVP delivery of CRISPR-Cas9 nucleases together with homology-directed repair templates tailored for HR or HMEJ achieves efficient and targeted insertion of large DNA cargoes (up to 14.8 kb) into *AAVS1*, a prototypic safe-harbor locus (56–58). Therapeutic gene knock-in into safe harbor loci is a flexible genome editing concept in that it offers the possibility for correcting recessive disease phenotypes independently of the underlying mutation(s); and the associated tools might, in principle, be directed to other conditions once validated in a specific setting. Additional versatility of this approach stems from the capacity to engineer AdVPs with CAR-independent fibers, whose engagement with alternative receptor(s) ensures efficient transduction of diverse human cell types (23,24). In this instance, targeted chromosomal integration of full-length dystrophin expression units in iPSCs and CAR-negative myoblasts was achieved using CD46-targeting AdVPs. This data raises the prospect for predictable and mutation-independent genetic complementa-

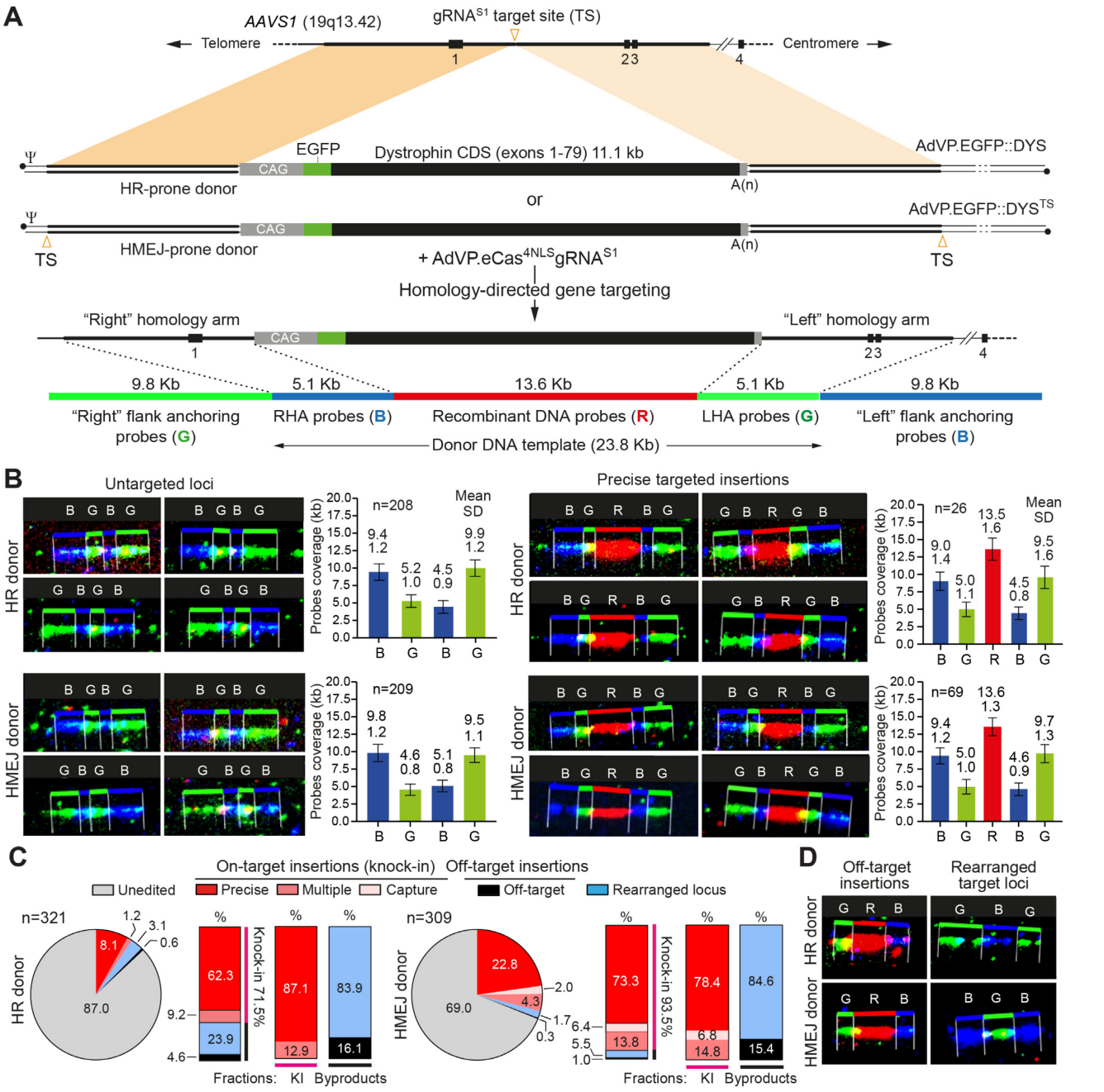

Figure 7. Establishing and characterizing AdVP-mediated targeted chromosomal insertion of large DNA at *AAVS1*. (**A**) Molecular combing set-up for measuring and mapping genome editing events. Schematic representation of homology-directed gene targeting substrates (i.e. donor DNA templates in AdVP.EGFP::DYS and AdVP.EGFP::DYS^{TS}) and precise DNA knock-in product triggered by gRNA^{S1}-directed DSB formation. The sizes and coverage of the probes used to stain recombinant DNA and genomic regions adjacent to the *AAVS1* target site are shown. G (green), 'right' flank anchoring probes or 'left' homology arm (LHA) probes; B (blue), 'Left' flank anchoring probes or 'right' homology arm (RHA) probes; R (red), recombinant DNA probes. (**B**) Validation of precisely targeted DNA insertions. Concordance between single-molecule measurements and theoretical values expected for precise genome editing events and unmodified target alleles in cell populations containing DMD.A myoblasts genetically modified with HR (8% EGFP::DYS^{+} cells) or HMEJ (34% EGFP::DYS^{+} cells) donor templates (top and bottom panels, respectively). The former and latter unselected myoblast populations were generated through co-transduction with AdVP.eCas9^{4NLS}gRNA^{S1} (10^4 GC cell^{-1}) and AdVP.EGFP::DYS (4 TU cell^{-1}) or AdVP.eCas9^{4NLS}gRNA^{S1} (10^4 GC cell^{-1}) and AdVP.EGFP::DYS^{TS} (4 TU cell^{-1}), respectively. The mean ± S.D. values (upper and lower numerals, respectively) correspond to the sizes (in kb) of the four *AAVS1* sections and the single recombinant DNA section hybridizing to the respective probes. The graphs were assembled by measuring the hybridization signals derived from the indicated numbers of individual fluorescently labelled loci. (**C**) Cumulative quantification of genome editing events. Absolute and relative molecular combing signal distributions (pie charts and parts of whole bars, respectively) corresponding to homology-dependent insertions (precise), multiple copy insertions and homology-independent insertions (capture) detected in unselected DMD.A myoblast populations containing stably transduced cells after delivery of AdVP.eCas9^{4NLS}gRNA^{S1} together with AdVP.EGFP::DYS (HR donor) or AdVP.EGFP::DYS^{TS} (HMEJ donor). (**D**) Detection of genome editing byproducts. Single-molecule detection of off-target DNA insertion events and rearranged target alleles in DMD.A myoblasts genetically modified with HR or HMEJ donor DNA delivered by AdVPs.

tion of patient-derived stem or progenitor cells with myogenic capability (28,29).

In the presence of CRISPR-Cas9 nucleases, HMEJ templates in AdVP genomes yielded higher frequencies of genome-edited cells than their HR counterparts in human myoblasts. Indeed, single-molecule visualization of exogenous and endogenous sequences by molecular combing revealed that chromosomal DNA insertions occurred mostly in a targeted and precise fashion. Unintended genome-editing events were nonetheless detected in the form of multiple or imprecise targeted insertions, off-target insertions, and on-target rearrangements. Hence, future research should be directed at identifying the parameters that minimize unwanted outcomes while further fostering precise gene targeting. A possibility concerns extending the homology arms in donor constructs beyond the current 10.2 kb of total target-donor DNA homology. Related to this, AdVP transduction experiments entailing the sole delivery of HR donors and positive/negative cell-selection regimens in iPSCs showed increased *CFTR* mutation correction frequencies via extending total target-donor homologies from 9.6 to 21.4 kb (18). In particular, homologies spanning 9.6 kb and 21.4 kb yielded 0.7×10^{-5} and 2.4×10^{-5} G418-resistant iPSCs (i.e. 3.4-fold increase), of which 75% and 100%, respectively, were shown to be correctly targeted after ganciclovir selection against random insertions (18). Of notice, recombinant DNA spanning 21–23 kb of target-site homologous sequences plus a full-length dystrophin expression unit 'fit' within AdVP capsids. The dual AdVP system investigated here should further allow identifying optimal dosages of each genome editing component by achieving efficient and segregated delivery of CRISPR-Cas9 nucleases and donor templates into different human cell types.

Adult stem or progenitor cells and reprogrammed iPSCs are particularly appealing targets for AdVP-assisted genome editing owing to the relevance of these cell types in the development of disease or synthetic biology models and candidate autologous cell therapies (63–65), such as those directed at striated muscle disorders (28,29,65). In this regard, earlier data showed that AdVP transduction of HR donors alone and together with *HBB*-specific TALENs yielded genome editing frequencies of 1.5×10^{-5} and 1.4×10^{-4}, respectively, as determined by counting G418-resistant iPSC clones originated from a sickle cell disease patient (i.e. 11-fold increment) (68). More recently, the enhancing effect of site-specific DSBs on AdVP-assisted iPSC genome editing was extended to the use of CRISPR-Cas9 nucleases. In particular, AdVP delivery of HR donors alone and together with *CFTR*-specific CRISPR-Cas9 complexes led to genome editing frequencies of 1.5×10^{-5} and 1.8×10^{-3}, respectively, as assessed by counting puromycin-resistant iPSC clones derived from a cystic fibrosis patient (i.e. 117-fold increment) (69).

In the present work, AdVP delivery of *AAVS1*-specific CRISPR-Cas9 nucleases and tailored HR templates yielded ∼0.1% and ∼1.0% of genome-edited DMD and wild-type iPSCs, respectively, as determined by reporter-directed flow cytometry and junction PCR assays, with the latter assay confirming HDR-derived gene knock-ins in randomly isolated iPSC clones. Crucially, these high frequencies of accurate genome-editing events were obtained using neither gene trapping nor positive/negative marker genes often necessary for selecting correctly targeted cell fractions (24).

DSBs, including those made by CRISPR nucleases, readily trigger p53-dependent cell cycle arrest and apoptosis in stem cells, which greatly hinders the recovery of cells precisely edited through HR (66,67). This outcome, shown to be aggravated in the presence of AAV donor constructs (67), can be alleviated through p53 inhibition (66,67). We found that after AdVP delivery, the normally higher CRISPR-Cas9-dependent genome editing levels achieved by engaging HMEJ over HR donors in muscle progenitor cells and HeLa cells are instead cancelled in iPSCs. Nevertheless, we report that the performance of iPSC genome editing involving HMEJ donor templates is rescued via p53 knockdown. These data suggest that gene knock-in strategies using such 'double-cut' donor designs might profit from transient p53 inhibition, especially so in highly DSB-sensitive cell types. Indeed, notwithstanding the risks associated with interfering with a key tumor suppressor protein, transient inhibition of p53 function at the post-transcriptional or post-translational levels is starting to be explored in stem and progenitor cells for enhancing precise HR-based gene knock-ins (67,70).

In conclusion, using DMD as a target disease model, we report that AdVPs constitute a robust platform for delivering and stably installing in a targeted homology-dependent manner large genetic payloads in human cells. Moreover, AdVPs serve as versatile probes for investigating the performance of different gene targeting approaches independently of genome-editing tool and donor DNA sizes.

DATA AVAILABILITY

All data gathered for and analyzed in this study are included in the article and supplementary files. The flow cytometry datasets were deposited at FlowRepository under accession codes FR-FCM-Z4SL, FR-FCM-Z4SX, FR-FCM-Z4SG, FR-FCM-Z4SF, FR-FCM-Z4SM, FR-FCM-Z4SP and FR-FCM-Z4SN. The amplicon deep sequencing library reads generated for this study were deposited at the NCBI Sequence Read Archive (SRA) database under BioProject ID PRJNA834963.

SUPPLEMENTARY DATA

Supplementary Data are available at NAR Online.

ACKNOWLEDGEMENTS

Authors of this paper are members of the European Reference Network – Neuromuscular diseases (ERN EURO-NMD). The authors thank Ignazio Maggio and Aart Jochemsen (Department of Cell and Chemical Biology, LUMC, Leiden, The Netherlands) for the generation of the *AAVS1*-targeting AdVP preparation and for providing the short-hairpin RNA constructs used in this study, respectively. The authors are also thankful to Vincent Mouly (Institute of Myology, Sorbonne University, Paris, France), Jacques Tremblay (Laval University Hospital Center, Quebec, Canada) and Stephen Hauschka (Department of Biochemistry, University of Washington, Seattle, USA) for sup-

plying wild-type and DMD myoblasts, the construct encoding the human full-length dystrophin, and the synthetic striated muscle-restricted CK8 promoter, respectively. Finally, the authors are grateful to all laboratory members for their support.

FUNDING

This project has received funding from the European Union's Horizon 2020 research and innovation programme under the Marie Skłodowska-Curie grant agreement no. 765269 (to F.T.). Prinses Beatrix Spierfonds [W.OR16-13]; Dutch Duchenne Parent Project [17.012]; China Scholarship Council–Leiden University Joint Scholarship programme (to Q.W.). Funding for open access charge: Prinses Beatrix Spierfonds.

Conflict of interest statement. None declared.

REFERENCES

1. Ernst,M.P.T., Broeders,M., Herrero-Hernandez,P., Oussoren,E., van der Ploeg,A.T. and Pijnappel,W. (2020) Ready for repair? gene editing enters the clinic for the treatment of human disease. *Mol. Ther. Methods Clin. Dev.*, **18**, 532–557.
2. Sharma,G., Sharma,A.R., Bhattacharya,M., Lee,S.S. and Chakraborty,C. (2021) CRISPR-Cas9: a preclinical and clinical perspective for the treatment of human diseases. *Mol. Ther.*, **29**, 571–586.
3. Cong,L., Ran,F.A., Cox,D., Lin,S., Barretto,R., Habib,N., Hsu,P.D., Wu,X., Jiang,W., Marraffini,L.A. *et al.* (2013) Multiplex genome engineering using CRISPR/Cas systems. *Science*, **339**, 819–823.
4. Cho,S.W., Kim,S., Kim,J.M. and Kim,J.S. (2013) Targeted genome engineering in human cells with the cas9 RNA-guided endonuclease. *Nat. Biotechnol.*, **31**, 230–232.
5. Jinek,M., East,A., Cheng,A., Lin,S., Ma,E. and Doudna,J. (2013) RNA-programmed genome editing in human cells. *Elife*, **2**, e00471.
6. Mali,P., Yang,L., Esvelt,K.M., Aach,J., Guell,M., DiCarlo,J.E., Norville,J.E. and Church,G.M. (2013) RNA-guided human genome engineering via cas9. *Science*, **339**, 823–826.
7. Kleinstiver,B.P., Pattanayak,V., Prew,M.S., Tsai,S.Q., Nguyen,N.T., Zheng,Z. and Joung,J.K. (2016) High-fidelity CRISPR-Cas9 nucleases with no detectable genome-wide off-target effects. *Nature*, **529**, 490–495.
8. Slaymaker,I.M., Gao,L., Zetsche,B., Scott,D.A., Yan,W.X. and Zhang,F. (2016) Rationally engineered cas9 nucleases with improved specificity. *Science*, **351**, 84–88.
9. Chen,X. and Gonçalves,M.A.F.V. (2018) DNA, RNA, and protein tools for editing the genetic information in human cells. *iScience*, **6**, 247–263.
10. Chandrasegaran,S. and Carroll,D. (2016) Origins of programmable nucleases for genome engineering. *J. Mol. Biol.*, **428**, 963–989.
11. He,X., Li,Y.X. and Feng,B. (2018) New turns for high efficiency knock-In of large DNA in human pluripotent stem cells. *Stem Cells Int.*, **2018**, 9465028.
12. Jang,H.K., Song,B., Hwang,G.H. and Bae,S. (2020) Current trends in gene recovery mediated by the CRISPR-Cas system. *Exp. Mol. Med.*, **52**, 1016–1027.
13. Zhang,J.P., Li,X.L., Li,G.H., Chen,W., Arakaki,C., Botimer,G.D., Baylink,D., Zhang,L., Wen,W., Fu,Y.W. *et al.* (2017) Efficient precise knockin with a double cut HDR donor after CRISPR/Cas9-mediated double-stranded DNA cleavage. *Genome Biol.*, **18**, 35.
14. Yao,X., Wang,X., Hu,X., Liu,Z., Liu,J., Zhou,H., Shen,X., Wei,Y., Huang,Z., Ying,W. *et al.* (2017) Homology-mediated end joining-based targeted integration using CRISPR/Cas9. *Cell Res.*, **27**, 801–814.
15. He,X., Tan,C., Wang,F., Wang,Y., Zhou,R., Cui,D., You,W., Zhao,H., Ren,J. and Feng,B. (2016) Knock-in of large reporter genes in human cells via CRISPR/Cas9-induced homology-dependent and independent DNA repair. *Nucleic Acids Res.*, **44**, e85.
16. Suzuki,K., Tsunekawa,Y., Hernandez-Benitez,R., Wu,J., Zhu,J., Kim,E.J., Hatanaka,F., Yamamoto,M., Araoka,T., Li,Z. *et al.* (2016) In vivo genome editing via CRISPR/Cas9 mediated homology-independent targeted integration. *Nature*, **540**, 144–149.
17. Byrne,S.M., Ortiz,L., Mali,P., Aach,J. and Church,G.M. (2015) Multi-kilobase homozygous targeted gene replacement in human induced pluripotent stem cells. *Nucleic Acids Res.*, **43**, e21.
18. Palmer,D.J., Grove,N.C., Ing,J., Crane,A.M., Venken,K., Davis,B.R. and Ng,P. (2016) Homology requirements for efficient, footprintless gene editing at the CFTR locus in human iPSCs with helper-dependent adenoviral vectors. *Mol. Ther. Nucleic Acids*, **5**, e372.
19. Yao,X., Wang,X., Liu,J., Shi,L., Huang,P. and Yang,H. (2018) CRISPR/Cas9-mediated targeted integration in vivo using a homology-mediated end joining-based strategy. *J. Vis. Exp.*, **133**, e56844.
20. Holkers,M., Maggio,I., Henriques,S.F., Janssen,J.M., Cathomen,T. and Gonçalves,M.A.F.V. (2014) Adenoviral vector DNA for accurate genome editing with engineered nucleases. *Nat. Methods*, **11**, 1051–1057.
21. Chen,X. and Gonçalves,M.A.F.V. (2016) Engineered viruses as genome editing devices. *Mol. Ther.*, **24**, 447–457.
22. Gonçalves,M.A.F.V. (2005) Adeno-associated virus: from defective virus to effective vector. *Virol. J.*, **2**, 43.
23. Gao,J., Mese,K., Bunz,O. and Ehrhardt,A. (2019) State-of-the-art human adenovirus vectorology for therapeutic approaches. *FEBS Lett.*, **593**, 3609–3622.
24. Tasca,F., Wang,Q. and Gonçalves,M.A.F.V. (2020) Adenoviral vectors meet gene editing: a rising partnership for the genomic engineering of human stem cells and their progeny. *Cells*, **9**, e953.
25. Ricobaraza,A., Gonzalez-Aparicio,M., Mora-Jimenez,L., Lumbreras,S. and Hernandez-Alcoceba,R. (2020) High-capacity adenoviral vectors: expanding the scope of gene therapy. *Int. J. Mol. Sci.*, **21**, e3643.
26. Duan,D., Goemans,N., Takeda,S., Mercuri,E. and Aartsma-Rus,A. (2021) Duchenne muscular dystrophy. *Nat. Rev. Dis. Primers*, **7**, 13.
27. Chemello,F., Bassel-Duby,R. and Olson,E.N. (2020) Correction of muscular dystrophies by CRISPR gene editing. *J. Clin. Invest.*, **130**, 2766–2776.
28. Boyer,O., Butler-Browne,G., Chinoy,H., Cossu,G., Galli,F., Lilleker,J.B., Magli,A., Mouly,V., Perlingeiro,R.C.R., Previtali,S.C. *et al.* (2021) Myogenic cell transplantation in genetic and acquired diseases of skeletal muscle. *Front. Genet.*, **12**, 702547.
29. Loperfido,M., Steele-Stallard,H.B., Tedesco,F.S. and VandenDriessche,T. (2015) Pluripotent stem cells for gene therapy of degenerative muscle diseases. *Curr. Gene Ther.*, **15**, 364–380.
30. Takahashi,K., Tanabe,K., Ohnuki,M., Narita,M., Ichisaka,T., Tomoda,K. and Yamanaka,S. (2007) Induction of pluripotent stem cells from adult human fibroblasts by defined factors. *Cell*, **131**, 861–872.
31. Mamchaoui,K., Trollet,C., Bigot,A., Negroni,E., Chaouch,S., Wolff,A., Kandalla,P.K., Marie,S., Di Santo,J., St Guily,J.L. *et al.* (2011) Immortalized pathological human myoblasts: towards a universal tool for the study of neuromuscular disorders. *Skeletal Muscle*, **1**, 34.
32. Cudré-Mauroux,C., Occhiodoro,T., Konig,S., Salmon,P., Bernheim,L. and Trono,D. (2003) Lentivector-mediated transfer of bmi-1 and telomerase in muscle satellite cells yields a duchenne myoblast cell line with long-term genotypic and phenotypic stability. *Hum. Gene Ther.*, **14**, 1525–1533.
33. Brescia,M., Janssen,J.M., Liu,J. and Gonçalves,M.A.F.V. (2020) High-capacity adenoviral vectors permit robust and versatile testing of DMD gene repair tools and strategies in human cells. *Cells*, **9**, 869.
34. Chen,X., Tasca,F., Wang,Q., Liu,J., Janssen,J.M., Brescia,M.D., Bellin,M., Szuhai,K., Kenrick,J., Frock,R.L. *et al.* (2020) Expanding the editable genome and CRISPR-Cas9 versatility using DNA cutting-free gene targeting based on in trans paired nicking. *Nucleic Acids Res.*, **48**, 974–995.
35. Zhang,M., D'Aniello,C., Verkerk,A.O., Wrobel,E., Frank,S., Ward-van Oostwaard,D., Piccini,I., Freund,C., Rao,J., Seebohm,G. *et al.* (2014) Recessive cardiac phenotypes in induced pluripotent stem cell models of jervell and lange-nielsen syndrome: disease mechanisms and pharmacological rescue. *Proc. Natl. Acad. Sci. U.S.A.*, **111**, E5383–E5392.

36. van den Berg,C.W., Ritsma,L., Avramut,M.C., Wiersma,L.E., van den Berg,B.M., Leuning,D.G., Lievers,E., Koning,M., Vanslambrouck,J.M., Koster,A.J. *et al.* (2018) Renal subcapsular transplantation of PSC-derived kidney organoids induces neo-vasculogenesis and significant glomerular and tubular maturation in vivo. *Stem Cell Rep.*, **10**, 751–765.
37. Chapdelaine,P., Moisset,P.A., Campeau,P., Asselin,I., Vilquin,J.T. and Tremblay,J.P. (2000) Functional EGFP-dystrophin fusion proteins for gene therapy vector development. *Protein. Eng.*, **13**, 611–615.
38. Gonçalves,M.A.F.V., Janssen,J.M., Nguyen,Q.G., Athanasopoulos,T., Hauschka,S.D., Dickson,G. and de Vries,A.A. (2011) Transcription factor rational design improves directed differentiation of human mesenchymal stem cells into skeletal myocytes. *Mol. Ther.*, **19**, 1331–1341.
39. Janssen,J.M., Liu,J., Skokan,J., Gonçalves,M.A.F.V. and de Vries,A.A. (2013) Development of an adeasy-based system to produce first- and second-generation adenoviral vectors with tropism for CAR- or CD46-positive cells. *J. Gene Med.*, **15**, 1–11.
40. Herold,M.J., van den Brandt,J., Seibler,J. and Reichardt,H.M. (2008) Inducible and reversible gene silencing by stable integration of an shRNA-encoding lentivirus in transgenic rats. *Proc. Natl Acad. Sci. U.S.A.*, **105**, 18507–18518.
41. Pelascini,L.P., Janssen,J.M. and Gonçalves,M.A.F.V. (2013) Histone deacetylase inhibition activates transgene expression from integration-defective lentiviral vectors in dividing and non-dividing cells. *Hum. Gene Ther.*, **24**, 78–96.
42. Pelascini,L.P. and Gonçalves,M.A.F.V. (2014) Lentiviral vectors encoding zinc-finger nucleases specific for the model target locus HPRT1. *Methods Mol. Biol.*, **1114**, 181–199.
43. Campostrini,G., Meraviglia,V., Giacomelli,E., van Helden,R.W.J., Yiangou,L., Davis,R.P., Bellin,M., Orlova,V.V. and Mummery,C.L. (2021) Generation, functional analysis and applications of isogenic three-dimensional self-aggregating cardiac microtissues from human pluripotent stem cells. *Nat. Protoc.*, **16**, 2213–2256.
44. Szuhai,K. and Tanke,H.J. (2006) COBRA: combined binary ratio labeling of nucleic acid probes for multi-color fluorescence in situ hybridization karyotyping. *Nat. Protoc.*, **1**, 264–275.
45. Conant,D., Hsiau,T., Rossi,N., Oki,J., Maures,T., Waite,K., Yang,J., Joshi,S., Kelso,R., Holden,K. *et al.* (2022) Inference of CRISPR edits from sanger trace data. *CRISPR J.*, **5**, 123–130.
46. Maggio,I., Holkers,M., Liu,J., Janssen,J.M., Chen,X. and Gonçalves,M.A.F.V. (2014) Adenoviral vector delivery of RNA-guided CRISPR/Cas9 nuclease complexes induces targeted mutagenesis in a diverse array of human cells. *Sci. Rep.*, **29**, 5105.
47. Wang,Q., Liu,J., Janssen,J.M., Le Bouteiller,M., Frock,R.L. and Gonçalves,M.A.F.V. (2021) Precise and broad scope genome editing based on high-specificity cas9 nickases. *Nucleic Acids Res.*, **49**, 1173–1198.
48. Wang,Q., Liu,J., Janssen,J.M., Tasca,F., Mei,H. and Gonçalves,M.A.F.V. (2021) Broadening the reach and investigating the potential of prime editors through fully viral gene-deleted adenoviral vector delivery. *Nucleic Acids Res.*, **49**, 11986–12001.
49. Martin,M. (2011) Cutadapt removes adapter sequences from high-throughput sequencing reads. *EMBnet. J.*, **17**, 10–12.
50. Clement,K., Rees,H., Canver,M.C., Gehrke,J.M., Farouni,R., Hsu,J.Y., Cole,M.A., Liu,D.R., Joung,J.K., Bauer,D.E. *et al.* (2019) CRISPResso2 provides accurate and rapid genome editing sequence analysis. *Nat. Biotechnol.*, **37**, 224–226.
51. Stirling,D.R., Swain-Bowden,M.J., Lucas,A.M., Carpenter,A.E., Cimini,B.A. and Goodman,A. (2021) CellProfiler 4: improvements in speed, utility and usability. *BMC Bioinf.*, **22**, 433.
52. Rossi,S., Szuhai,K., Ijszenga,M., Tanke,H.J., Zanatta,L., Sciot,R., Fletcher,C.D.M., Tos,A.P.D. and Hogendoorn,P.C.W. (2007) *EWSR1-CREB1* and *EWSR1-ATF1* fusion genes in angiomatoid fibrous histiocytoma. *Clin. Cancer Res.*, **13**, 7322–7328.
53. Gonçalves,M.A.F.V. and de Vries,A.A. (2006) Adenovirus: from foe to friend. *Rev. Med. Virol.*, **16**, 167–186.
54. Gaggar,A., Shayakhmetov,D.M. and Lieber,A. (2003) CD46 is a cellular receptor for group b adenoviruses. *Nat. Med.*, **9**, 1408–1412.
55. Gonçalves,M.A.F.V., Holkers,M., Cudre-Mauroux,C., van Nierop,G.P., Knaan-Shanzer,S., van der Velde,I., Valerio,D. and de Vries,A.A. (2006) Transduction of myogenic cells by retargeted dual high-capacity hybrid viral vectors: robust dystrophin synthesis in duchenne muscular dystrophy muscle cells. *Mol. Ther.*, **13**, 976–986.
56. Papapetrou,E.P. and Schambach,A. (2016) Gene insertion into genomic safe harbors for human gene therapy. *Mol. Ther.*, **24**, 678–684.
57. Pavani,G. and Amendola,M. (2020) Targeted gene delivery: where to land. *Front. Genome Ed.*, **2**, 609650.
58. Lombardo,A., Cesana,D., Genovese,P., Di Stefano,B., Provasi,E., Colombo,D.F., Neri,M., Magnani,Z., Cantore,A., Lo Riso,P. *et al.* (2011) Site-specific integration and tailoring of cassette design for sustainable gene transfer. *Nat. Methods*, **8**, 861–869.
59. Slaymaker,I.M., Gao,L., Zetsche,B., Scott,D.A., Yan,W.X. and Zhang,F. (2016) Rationally engineered cas9 nucleases with improved specificity. *Science*, **351**, 84–88.
60. Maggio,I., Zittersteijn,H.A., Wang,Q., Liu,J., Janssen,J.M., Ojeda,I.T., van der Maarel,S.M., Lankester,A.C., Hoeben,R.C. and Gonçalves,M.A.F.V. (2020) Integrating gene delivery and gene-editing technologies by adenoviral vector transfer of optimized CRISPR-Cas9 components. *Gene Ther.*, **27**, 209–225.
61. Dang,Y., Jia,G., Choi,J., Ma,H., Anaya,E., Ye,C., Shankar,P. and Wu,H. (2015) Optimizing sgRNA structure to improve CRISPR-Cas9 knockout efficiency. *Genome Biol.*, **16**, 280.
62. Bonini,C., Grez,M., Traversari,C., Ciceri,F., Marktel,S., Ferrari,G., Dinauer,M., Sadat,M., Aiuti,A., Deola,S. *et al.* (2003) Safety of retroviral gene marking with a truncated NGF receptor. *Nat. Med.*, **9**, 367–369.
63. Tolle,F., Stucheli,P. and Fussenegger,M. (2019) Genetic circuitry for personalized human cell therapy. *Curr. Opin. Biotechnol.*, **59**, 31–38.
64. Sharma,A., Sances,S., Workman,M.J. and Svendsen,C.N. (2020) Multi-lineage human iPSC-derived platforms for disease modeling and drug discovery. *Cell Stem Cell*, **26**, 309–329.
65. Campostrini,G., Windt,L.M., van Meer,B.J., Bellin,M. and Mummery,C.L. (2021) Cardiac tissues from stem cells: new routes to maturation and cardiac regeneration. *Circ. Res.*, **128**, 775–801.
66. Ihry,R.J., Worringer,K.A., Salick,M.R., Frias,E., Ho,D., Theriault,K., Kommineni,S., Chen,J., Sondey,M., Ye,C. *et al.* (2018) p53 inhibits CRISPR-Cas9 engineering in human pluripotent stem cells. *Nat. Med.*, **24**, 939–946.
67. Schiroli,G., Conti,A., Ferrari,S., Della Volpe,L., Jacob,A., Albano,L., Beretta,S., Calabria,A., Vavassori,V., Gasparini,P. *et al.* (2019) Precise gene editing preserves hematopoietic stem cell function following transient p53-Mediated DNA damage response. *Cell Stem Cell*, **24**, 551–565.
68. Suzuki,K., Yu,C., Qu,J., Li,M., Yao,X., Yuan,T., Goebl,A., Tang,S., Ren,R., Aizawa,E. *et al.* (2014) Targeted gene correction minimally impacts whole-genome mutational load in human-disease-specific induced pluripotent stem cell clones. *Cell Stem Cell*, **15**, 31–36.
69. Palmer,D.J., Turner,D.L. and Ng,P. (2020) A single "All-in-One" helper-dependent adenovirus to deliver donor DNA and CRISPR/Cas9 for efficient homology-directed repair. *Mol. Ther. Methods Clin. Dev.*, **17**, 441–447.
70. Lee,B.C., Lozano,R.J. and Dunbar,C.E. (2021) Understanding and overcoming adverse consequences of genome editing on hematopoietic stem and progenitor cells. *Mol. Ther.*, **29**, 3205–3218.